Field Theory Coefficients For Ising Surface Criticality

by

Dorian Przetakiewicz

Aachen, 8^{th} of March 2024

A Bachelor's Thesis

First Examiner: Prof. Dr. Stefan Weßel,
Second Examiner: Prof. Dr. Moritz Julian Helias,
Supervisor: Priv. Doz. Dr. Francesco Parisen Toldin

Institute for Theoretical Solid-State Physics at RWTH University Aachen

Acknowledgements

Completing this thesis would have been unattainable without the support of my supervisor Priv. Doz. Francesco Parisen Toldin. Thank you Francesco, for your time as well as all the help, guidance, and explanations you provided me with. Prof. Dr. Stefan Wessel has given me the possibility to write this thesis. Thank you very much Stefan for opening the door to this project and allowing me write this thesis.

Simulations were performed with computing resources granted by RWTH Aachen University under project thes1638 and the cluster 'theophysc'.

Contents

1 Introduction

The invention of the computer has clearly changed our world. Advances in technology are happening so rapidly that it is becoming increasingly difficult to keep track of these advances. The computer has brought about an incredible new world of possibilities, especially in the world of physics. Be it experimental or theoretical physics, computers are now indispensable and enable us to conduct research at a whole new level.
In the field of theoretical solid state physics, they are used for Monte Carlo simulations, among other things. They allow us to study complex - sometimes analytically *nonsolvable-systems* through the use of statistics and random number generation.
Monte Carlo simulations have their origins in the 18th century, when Georges Louis Leclerc, Comte de Buffon, developed a method to approximate π by throwing needles onto two parallel boards lying on top of each other. The ratio of needles on both boards determined this approximation. The real beginning of the development of Monte Carlo simulation was in 1940, when von Neumann and Ulam considered how they could model neutron transport. This was done on the first computer designed for this purpose, called the *Fermiac*[13].
Here we use a Monte Carlo simulation to simulate our system, which in our case can be described by a Hamiltionan $\hat{\mathcal{H}}$, under certain conditions. The point, however, is that no matter what sequence of random numbers we use, the result should be the same within an uncertainty if we used a different sequence of random numbers.
To be more precise, a major part of this thesis is the simulation of the Blume-Capel model in 3D. This model is considered at a critical temperature T_c. One can imagine it as a cube with many grid points, where each point on the grid takes the value of a spin, -1, 0 or 1. There are then so-called *open* or *periodic* boundary conditions. These decide if our system contains surfaces. We are interested in both cases.
In the chapter **Boundary Critical Phenomena**, the theory involved is discussed in more detail. First, I explain the two different types of phase transitions in general, then I discuss the emergence of *critical exponents* near the critical temperature T_C. I then convey the concept of *universality*, which explains the linking of different systems that exhibit similar behavior at the critical point. This concept is then discussed in more detail regarding the context of surfaces. Ultimately, however, the aim of this thesis is to determine the amplitudes of three correlation functions. In the field-theoretical formulation of these correlations, a boundary operator product expansion coefficient μ can be calculated based on these amplitudes. This coefficient is universal. The results of this will be presented in chapter five, while in chapter four I will explain my progress towards creating a valid simulation of this model and give details on the Monte Carlo algorithm and the algorithms used within it.

2 Definitions

Here I will briefly denote a few definitions, used in this thesis:

1. $\mathcal{J}$ is defined as the coupling constant. In this thesis, the value of $\mathcal{J}$ is set to one at all times where numerical simulations are performed

$$\mathcal{J} = 1. \tag{1}$$

   As $\mathcal{J}$ has the dimension of energy, and numerical simulation can only be done on dimensionless quantities, by setting $\mathcal{J}$ to 1 we *remove* this dimension from our model and thus can perform numerical simulations seamlessly. The consequence is that the temperature T (and β) become dimensionless as well.
   Following the same logic, I set the Boltzmann constant $k_B = 1$ as well, so that generally $\beta = 1/T$.

2. T_C is called critical temperature, at this temperature a system is said to be *critical* which means that it is on the verge of undergoing a phase transition.

3. β_c is defined as the inverse critical temperature of a system. It is defined as

$$\beta_C = \frac{1}{T_C}. \tag{2}$$

4. *Criticality* - A system *approaching criticality* means that it is within close vicinity to the critical point β_c. At criticality means exactly at $\beta = \beta_c$.

3 Boundary Critical Phenomena

Critical phenomena are observed at second-order (continous) phase transitions. The effects range from the so-called *critical slowing down* up to the divergence of the correlation length ξ or the existence of critical exponents. Strangely enough critical exponents can be the same for a variety of different systems, for example the transition of heating up water (liquid-gas transition) and the transition between the paramagnetic and ferromagnetic phase of for example iron. This phenomenon is called *universality*. This and the more specific topic of *surface universality* will be discussed in this section.

3.1 Phase Transitions

A phase transition is the transition of a physical system's current state to another. This process can be detected by sudden change in value of an *order parameter*. One such order parameter is for example the spontaneous magnetization of a ferromagnet. In the *ordered* phase its value is non-zero, while in the *disordered* state it is zero. In the case of the Ising model (which represents a ferromagnet), this transition happens at a (inverse) temperature $\beta_{c,Ising}$. That

means if we approach this inverse temperature by cooling our system down, it will transition from the disordered state ($\beta < \beta_{c,Ising}$) to the ordered state ($\beta > \beta_{c,Ising}$) upon crossing $\beta_{c,Ising}$.
Phase transitions can be differentiated between first-order and second-order transitions. The difference between them is that for first-order transitions the derivative of the free energy is *discontinous* at the critical temperature T_c, while for second-order transitions the derivative is *continous* and the second derivative of the free energy contains singularities[13].
The correlation length ξ is defined as the typical scale of length over which we notice a correlation in the fluctuations of the microscopic degrees of freedom in a system. Systems that undergo a second-order transition exhibit a divergence in the correlation length ξ at the critical point, and near the critical point the correlations exhibit a power-law-like behaviour. In contrary, systems undergoing a first-order transition exhibit a finite correlation length ξ at the transition temperature. This means that for example a ferromagnet at the critical point, which undergoes a second-order transition, is in a unique - critical state because the fluctuations are correlated over all distances, and thus the transition happens 'smoothly' - in a continous matter. In the case of a first-order phase transition the two phases ($\beta \lessgtr \beta_{c,Ising}$) would coexist at the critical point[20]. In this thesis, our system undergoes a second-order phase transition at β_c.

3.2 Critical exponents

Near a critical point, thermodynamic properties such as the order parameter m for a ferromagnet exhibit behavior that follows a power-law[13]:

$$m = m_0 \tau^{\beta} \tag{3}$$

with $\tau = |1 - \frac{T}{T_c}|$.[1] The critical amplitudes (in this case m_0) may differ if the critical temperature is approached from $T \to T_c^+$ or $T \to T_c^-$. Generally these critical exponents are not exact numbers, this is only the case for a very small amount of models - for example the 2D Ising model, which was solved analytically by L. Onsager in 1944[16]:

1. $\alpha = 0$
2. $\beta = \frac{1}{8}$
3. $\gamma = \frac{7}{4}$

The exponent $\alpha = 0$ corresponds to the (logarithmic) divergence of the specific heat, β to the magnetization and γ to the susceptibility[13]. Using Monte Carlo simulations, these critical exponents can be approximated for a variety of systems whose critical exponents can not be found analytically.

[1] It is important to note that the critical exponents may be different above and below the critical temperature in some cases[14].

3.3 Universality

Some systems, as different as they appear to be, may have the same set of critical exponents. In that case critical exponents of some arbitrarily complex system might be found by determining the same exponents but using a different model. This is possible if both of these systems lie in the same 'universality class'. An example for this would be the Ising model and the Blume Capel model with periodic boundaries (bulk transition), which are part of the Ising universality class[9].
It is even possible for a quantum and a classical system to be in the same universality class, for example the liquid-gas transition and the paramagnetic-ferromagnetic transition of iron. This means that studying the transition in the Ising model, teaches us something about the liquid-gas transition. To further elaborate on this, I summarised Prof. Dr. B. Simons lecture notes on this example [20]:
Usually magnetic transitions are observed to be second-order phase transitions, as in the case of the Ising model. The liquid-gas transition corresponds to a first-order phase transition because at the boiling point, the systems entropy $Q_L = T_C \Delta S$ jumps discontinuously due to the absorption of latent heat coming from vapourisation. This happens due to the fact that the temperature of the system stays constant until the whole system has transitioned into the gaseous phase, but the absorption of the latent heat still takes place. This shows up in a change in entropy. How can these systems have something in common?
The behaviour I just described is just one specific path in which the transition can take place for these systems. If we look at Fig. 1 (a) we can see the phase transition of a ferromagnet with external field $H = 0$ ($b \to c \to d$). The Point c marks the critical point. This is where the continous phase transition happens ($T = T_C$), the average magnetisation begins to grow from zero at $T > T_C$ to a non-zero value for $T < T_C$.
In the case of the liquid-gas transition at constant pressure, see Fig. 1 (b), we find the first-order phase transition, where a discontinous change in density happens as we cross the line ($b' \to c' \to d'$).
Both of these transitions are not really comparable, but if we take a look at the transition that takes place when varying H at $T < T_C$, we find similar behaviour to the liquid-gas transition with constant pressure. This can be seen in Fig. 1 (c) where the magnetisation jumps discontinuously to a positive value if H passes through 0^+ ($b' \to c' \to d'$).
In the case of the liquid, we find the transition in Fig. 1 (d) to be comparable with (a). When the density of the fluid is fixed at its critical value ρ_c, the transition is of second-order and thus resembles the ferromagnetic transition for $H = 0$ ($b \to c \to d$).
This is an example of universal behaviour. Both systems belong to the same universality class, because they exhibit similar behaviour while undergoing a phase transition. There are many properties that help in determining the universality class, for example the range of interaction, symmetry of the ordered state and more[13]. The most powerful characteristic is that both systems can

be described by the same set of critical exponents!

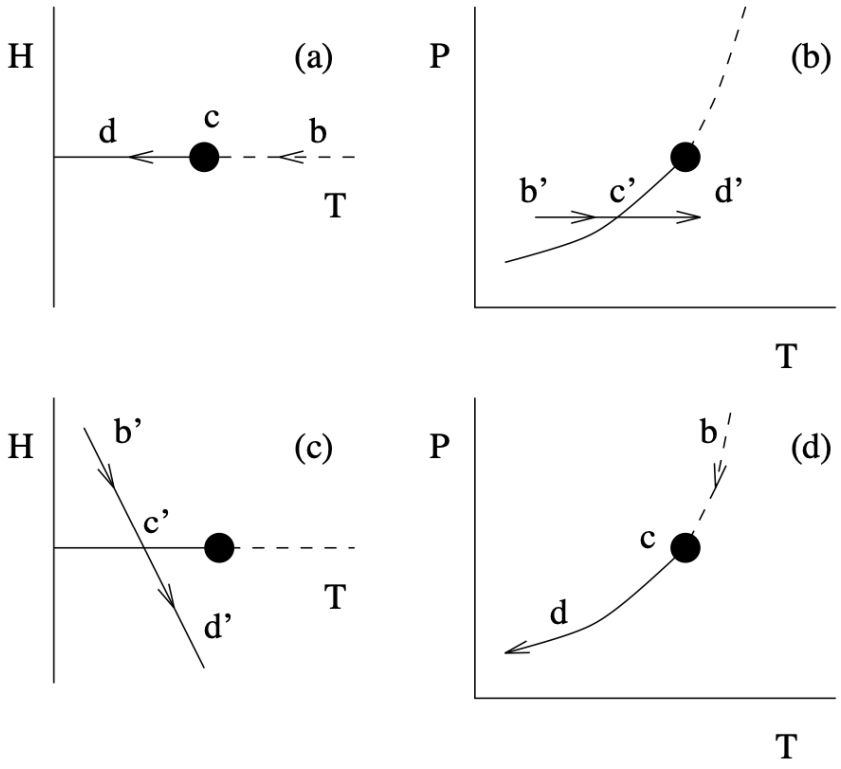

Figure 1: The liquid-gas transition compared to the ferromagnetic phase transition in the Ising model. Image taken from lecture on Critical Phenomena by Prof. Dr. B. Simons [20], can be found here: https://www.tcm.phy.cam.ac.uk/∼bds10/phase/introduction.pdf

One important remark: The models inside a universality class differ at finite scales. This is due to so called *finite size effects*. These effects are something we have to deal with in numerical simulations because we can not just simulate infinite lattices. But in the limit $L \to \infty$ the models become increasingly similar, because microscopic short-distance correlations become dominated by the long-distance macroscopic correlations since the correlation length ξ diverges at the critical point. In order to calculate meaningful results in our simulation, we include a correction term that covers the finite size effects.

3.4 Renormalization group idea

This section is based on chapter three from the book "Scaling and Renormalization in Statistical Physics" by John Cardy[6]. The idea of the renormalization group procedure can be simply understood with the *coarse graining* of the Ising model. Imagine a two-dimensional Ising lattice. The spins are either pointing up or down ($s = \pm 1$). Now we execute *block spin transformations*. This means we group the spins into 3 x 3 blocks, where each block contains exactly nine spins. *Coarse graining* now means that we transform each of these blocks of spins into new single spins s'. The way one could perform the transformation is for example by using the *majority rule*, where the new spin of some block $s' = \pm 1$ is determined by whichever spin has the majority in the given block. If we think of this procedure in a visual way, it would be equivalent to rescaling a picture down to a worse resolution, where we combine nine pixels into a single pixel. Put it simply - we lose detail. The catch is however, that for systems at the critical point, each new configuration obtained through repeated blocking, regardless of the number of iterations, is statistically identical to the original one. This is also called *scale invariance*.
The underlying assumption of the renormalization group is that no matter how often we iterate through this transformation, the dominant interactions will always be short-ranged. One can prove that the partition function of the initial system and the blocked system is the same:

$$\mathrm{Tr}_s \, e^{-\mathcal{H}(s)} = \mathrm{Tr}_{s'} \, e^{-\mathcal{H}'(s')} \tag{4}$$

where $\mathcal{H}'(s')$ denotes the Hamiltonian of the *blocked system*[6]. It is important to note, that in these (*reduced*) Hamiltonians β is absorbed inside the other parameters, for example the exchange coupling $\mathcal{J}$, so the (*reduced*) coupling is $K = \beta\mathcal{J}$.
However the consequences of Eq. 4 go much further. The probability distribution of observables that only depend on (blocked) spins s', s'',... will be left invariant at higher levels of blocking and so the large distance physics will remain untouched by this procedure.
One must keep in mind that $\mathcal{H}'(s')$ will generally contain a renormalized value of the coupling K, denoted K'. In the case of the 1D Ising model this would look like:

$$\mathcal{H}'(s') = Ng(K, K') - K' \sum_i s'_i s'_{i+1} \tag{5}$$

where N is the total number of original sites and $g(K, K')$ some function depending on K and K'[6]. The term $Ng(K, K')$ has no influence on the calculation of the expectation values of any observables, but it does have an influence on the free energy. It will become the inhomogenous term inside of it (Eq. 7), which in our case will be irrelevant. Here we are only interested in the singular behaviour of the free energy as I will discuss in the next section about scaling forms.

3.4.1 Scaling Forms

Scaling forms describe how observables like e.g. the susceptibility χ or the magnetization m change when the system approaches criticality and how external parameters like the temperature or magnetic field influence this behaviour.
A homogenous function of degree k is a function for which the following relation is true:

$$p(s \cdot x) = s^k p(x). \tag{6}$$

Extensive variables like the free energy can usually be expressed by homogenous functions[1]. However in the case of systems treated using the renormalization group procedure, the free energy generally has an inhomogenous term:

$$f = f_{inh.} + f_{hom.}. \tag{7}$$

Here we are only interested in the singular behaviour of the free energy, which corresponds to the homogenous part. For this reason we drop the inhomogenous term[6]. In particular the singular form of the free energy can be expressed in the following homogenous form[21]:

$$f_{sing}(\tau, h) = \tau^{2-\alpha} g_f \left(\frac{h}{\tau^{\Delta}} \right). \tag{8}$$

This equation makes sense considering the following proportionality:

$$C \propto -\frac{\partial^2 f}{\partial \tau^2}. \tag{9}$$

Near the critical (singular) point, the heat capacity follows a power-law behaviour with the critical exponent α:

$$C = C_0 \tau^{-\alpha} \tag{10}$$

using Eq. 8 and Eq. 9 we find Eq. 10 for $h = 0$ through differentiation ($g_f(0) = const$ per definition). So the formula for the singular form of the free energy is chosen such that it reproduces the heat capacity singularity (Eq. 10). How does this work in the case of $h \neq 0$?
Consider

$$E_{sing} \propto \frac{\partial f}{\partial \tau} \propto (2-\alpha)\tau^{1-\alpha} g_f \left(\frac{h}{\tau^{\Delta}} \right) - \Delta h \tau^{1-\alpha-\Delta} g_f' \left(\frac{h}{\tau^{\Delta}} \right), \tag{11}$$

since the derivative of a homogenous function is another homogenous function[21], we can rewrite Eq. 11 as:

$$E_{sing} \propto \frac{\partial f}{\partial \tau} = \tau^{1-\alpha} \left[(2-\alpha) g_f \left(\frac{h}{\tau^{\Delta}} \right) - \frac{\Delta h}{\tau^{\Delta}} g_f' \left(\frac{h}{\tau^{\Delta}} \right) \right] \equiv \tau^{1-\alpha} g_E \left(\frac{h}{\tau^{\Delta}} \right), \tag{12}$$

where $g_E\left(\frac{h}{\tau^\Delta}\right)$ is the new *scaling function* of E_{sing}. If we take the derivative again, we get the heat capacity and we apply the same idea again:

$$C_{sing} \propto -\frac{\partial^2 f}{\partial \tau^2} \propto \tau^{-\alpha} g_C\left(\frac{h}{\tau^\Delta}\right). \tag{13}$$

This works for other observables like the magnetization or susceptibility as well[21].
Now what is $g_f(\frac{h}{\tau^\Delta})$?
This is a *scaling function*. It describes how f_{sing} scales with h and τ, where its magnitude increases near the critical point. This equation is interesting if $h \neq 0$ since if $h = 0$ we simply get the power-law behaviour of the heat capacity (Eq. 10). So in other words - for example $g_C(\frac{h}{\tau^\Delta})$ rescales the heat capacity if there is some external field h applied. The most important fact about it is, that this behaviour is universal[6]. The exponent Δ is called the *gap exponent*. This exponent Δ as well as α depend on the critical point which is being considered.

3.5 Surface effects

The following two sections are mainly based on H. W. Diehl's paper on the "Theory of Boundary Critical Phenomena", where he discusses surface effects, surface universality classes and the three important types of phase transitions in that regard[7].
Two very important properties that are usually dismissed are the *finite size* and presence of *surfaces*, when studying models near the critical point. While the effects arising from the *finite size*, are called *finite size effects*, there are also effects arising with the presence of surfaces called *boundary effects*. In the following I will discuss the possible boundary effects.
One is, that when we look at some order parameter, the behaviour of it in regions near the surface *differs* in comparison to its behaviour inside the bulk. The thickness of these regions is proportional to the correlation length ξ. That means we find e.g. the magnetization to be *inhomogenous* inside the system on the scale of ξ *near* the surface[7]. This behaviour is visualised for $T < T_C$ and $\xi \ll L$ in Fig. 2. We clearly see that deep in the bulk, the value of the magnetization approaches the bulk magnetization m_b, up to corrections $\propto \exp(-\frac{z}{\xi})$, and it is just nearby the surfaces that we see the local densities to deviate from m_b.
Another consequence arises when we integrate over some density.
For example in the case of the magnetization in the region occupied by the system[2] $\mathcal{M} \subset \mathbb{R}^3$:

$$\frac{1}{V}\int_{\mathcal{M}} d^3x\, m(x) \approx m_b + \frac{A}{V} m_s + \mathcal{O}(L^{-2}) \tag{14}$$

for $L \to \infty$, with $\frac{A}{V} = \frac{L^2}{L^3}$. This equation denotes the magnetization per volume, and is here an integral because the limit $L \to \infty$ is taken. Contributions

[2]For simplicity and because this thesis covers a 3D model, I have decided not to generalise the formulas to d-Dimensions but stick with d = 3 here.

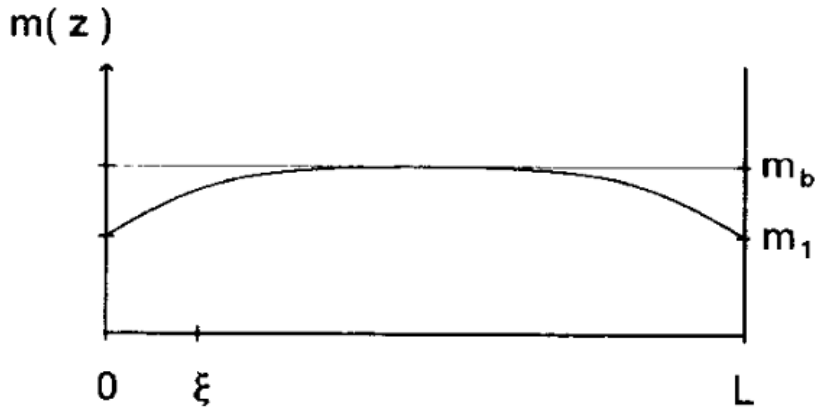

Figure 2: The behaviour of the magnetization between two parallel surfaces, distanced with the length L in z-direction, $\xi \ll L$ and $T < T_C$. The effects of other possible surfaces are neglected and m_b stands for the bulk magnetization. Image found on page 4 of Diehl's paper[7].

$\propto L^{-2}$ or smaller are neglected here. The quantity m_s is the *surface excess magnetization*. The decomposition of $m \to m_s$, m_b can be done for other quantities as well.
Generally the term regarding the surface corrections inside Eq.14 is small when L is large and $\xi \ll L$. Although if we begin to approach the critical point (from below) with our *finite* system, the correlation length approaches the order of L. This is when our system becomes more and more correlated and even the spins on opposite surfaces show a non-zero correlation. At this point the decomposition into bulk and surface contributions does not make sense anymore. When approaching the critical point, the correlation length ξ spreads differently near the surface than it does in the bulk because the surface has a different dimension than the bulk. This means that m_s can approach zero at a different rate than m_b which is definitely zero at the critical point. The reason is that the m_s is dependent on the surface enhancement parameter c that I will introduce later. So boundary effects become irrelevant and finite-size effects come into play. In order to eliminate the finite-size effects one can take the thermodynamic limit ($L \to \infty$) first and then approach the critical point.
When this is done, one can find power-law like behaviour of the bulk densities near the critical point (as in Eq. 3) in the case of no external magnetic field:

$$m_b \approx M_+ \tau^\beta, \; as \; T \to T_C^+ \tag{15}$$

and for the singular part of the bulk free energy f_b:

$$f_b^{sing} \approx B_\pm \tau^{2-\alpha}, \; as \; T \to T_C^\pm, \tag{16}$$

where α and β are standard critical exponents and M_+ and $B_\pm$ *nonuniversal* amplitudes.
Now if we consider some region near a surface, precisely within a distance $z \ll \xi$, we can expect that some quantity like the magnetization will display power-law like behaviour near the critical point. But due to the presence of boundary effects, the critical exponents can generally be *different* than in the bulk:

$$m(z=0) \propto \tau^{\tilde{\beta}},\ as\ T \to T_C^+. \tag{17}$$

This means there must be a new type of universality class that contains these new critical exponents. This leads to the idea of having a set of *bulk universality classes* that includes the *bulk critical exponents* and a set of *surface universality classes* that include the critical exponents that characterize the behaviour of local quantities near surfaces. It can be shown that generally for a given *bulk universality class* there exist several distinct *surface universality classes*[7].

3.6 Surface universality classes

As previously mentioned in the chapter on the idea of renormalization, we assume that the dominant interactions are always short-ranged. This must hold true in these types of systems as well at any point, whether in the bulk or near a surface.
Now it is important to remark, that the boundary effects *must* be of short-range as well. So any contributions to these interactions, created by the surface must have a short range.
Generally there are three phases we can find our system in:

1. surface-ordered / bulk-disordered (SO/BD)
2. surface-disordered / bulk-disordered (SD/BD)
3. surface-ordered / bulk-ordered (SO/BO)

A phase of type (SD/BO) is not found because if the bulk would be ordered, it would act like an external field on the surface and would thus order it. The phase diagram of the semi-infite *n-vector model* or simply $O(n)$ model where these three states are shown, can be seen in Fig. 3. For example in the case $O(1)$, this model would be equivalent to the Ising model.
We notice the parameter $-c$ on the horizontal axis. The parameter c_0 corresponds to the *surface enhancement* and is a constant that arises in the field theoretical formulation of this model. The parameter c is proportional to it,

$$c \propto c_0 - c_{sp} \tag{18}$$

with c_{sp} chosen such that the point **Sp** is located at $c = 0$. The point **Sp** is a *multicritical* point, where the phase transition lines meet and it describes the *special transition*. There are three other transitions, as seen on the labels of the lines:

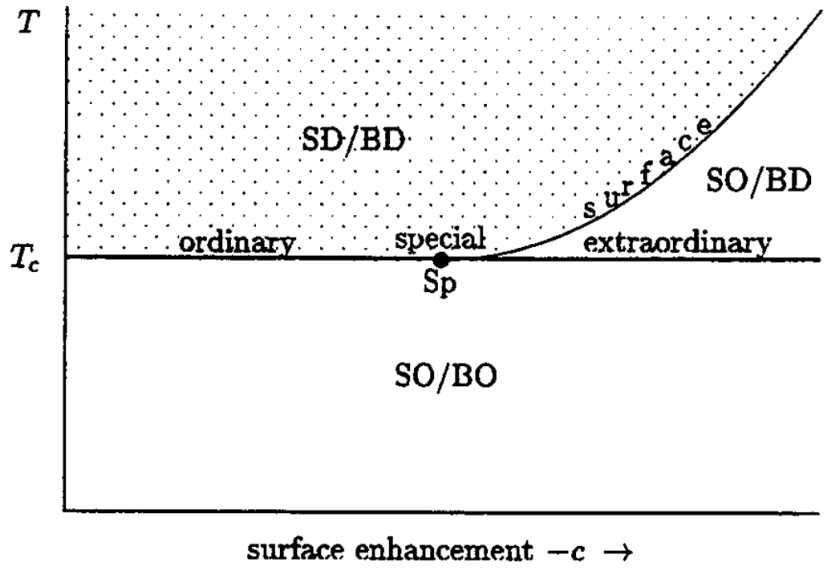

Figure 3: The phase diagram of the semi-infite *n-vector model*. Image found on page 8 of Diehl's paper[7].

1. the ordinary transition
2. the surface transition
3. the extraordinary transition

where each of these three transitions, including the special transition, are of second-order[7].

3.6.1 The ordinary transition

The ordinary transition takes place when the surface enhancement parameter is subcritical $c > 0$ and the temperature is lowered. In this case the surface transitions from disordered $\rightarrow$ ordered and the bulk from disordered $\rightarrow$ ordered; (SD/BD) $\rightarrow$ (SO/BO).
The ordinary transition of the Blume-Capel model is the transition I am studying in this thesis.

3.6.2 The surface transition

The surface transition takes place, when the surface enhancement parameter is supercritical $c < 0$ and the temperature is lowered to a value $T > T_C$. The system then undergoes a phase transition where only the surface transitions from

disordered → ordered; (SD/BD) → (SO/BD). This transition is equivalent to a two-dimensional bulk transition.

3.6.3 The extraordinary transition

The extraordinary transition takes place at the same conditions as the surface transition, $c < 0$, but the value of the temperature is lowered across the critical point $T < T_C$.

3.6.4 The special transition

The special transition takes place when the surface enhancement parameter is critical, $c = 0$ and the temperature is lowered through the critical point T_C, and thus across the special point **Sp**.

4 Model and simulation

In the following section the code I am referring to, was written by myself as part of this thesis[3]. Although in the determination of the amplitudes later, the code from my supervisor Dr. Francesco Parisen Toldin has been used, which he gave me permission to. The Monte Carlo parameters used in his simulation differ slightly in comparison to mine, I will discuss the differences in a later section before discussing the results.

4.1 The 3D Blume-Capel model

We consider the Blume-Capel Model in 3D. It is characterized by the reduced Hamiltonian[3][5]

$$\hat{\mathcal{H}} = -\beta \sum_{<xy>} s_x s_y + D \sum_x s_x^2 - h \sum_x s_x. \tag{19}$$

The x and y denote a site of the lattice here, $x = (x_1,\ x_2,\ x_3)$ where each component x_i or y_i take a value ranging from $1 \leq x_i \leq L_i$. Thus in the first sum, the $< xy >$ means a sum over nearest neighbours inside the 3D cube. In the case of periodic boundaries on finite lattices, we consider the spin on the opposite site as next neighbour when the spin s_x lies on a surface or a corner. In the Blume-Capel model the possible values for the spins s_x are $s_x = \{-1, 0, 1\}$. The parameter h stands for the external field, although in this thesis we consider a vanishing field of $h = 0$. Lastly the parameter D controls the density of spins equal to zero ($s_x = 0$). That means if we consider the limit $D \to -\infty$ we will recover the simple Ising model with the Hamiltonian (for $h = 0$) because the density of spins $s_x = 0$ becomes fully surpressed

[3]Link to my Code: https://github.com/spyder73/Blume-Capel-3D

$$\lim_{D\to-\infty} \hat{\mathcal{H}}|_{h=0} \to \hat{\mathcal{H}}_{Ising}|_{h=0} = -\beta \sum_{<xy>} s_x s_y. \tag{20}$$

The Blume-Capel model lies in the 3D Ising bulk universality class. In the case of open boundaries, this system lies in the ordinary surface universality class at the point β_c, which is a sub-class of the 3D Ising bulk universality class.

4.1.1 Monte Carlo parameters

At the critical point we are looking at, the amplitude of leading corrections to scaling vanishes for a choice of $D = 0.655$. The corresponding (inverse) critical temperature (also called critical coupling, because $\mathcal{J}$=1) for this is found to be[9]:

$$\beta_c(0.655) = 0.387721735(25) \tag{21}$$

This point (D, $\beta_c(D)$) corresponds to a point on the line of second-order phase transition, specifically in the region of the ordinary transition. For the generation of pseudo-random numbers I used the Mersenne Twister algorithm in all simulations[19]. For each lattice size L, the simulation runs for 10.000 Monte Carlo steps. Inside each of these steps I run the Metropolis algorithm for L^3 steps and the Wolff algorithm right after that for L steps. We assume that it takes a while for the system to become thermalized, thus we discard the results of the first 2000 Monte Carlo steps (20%) and use the 8000 remaining ones for our calculations. The data is then grouped in N_{Bin} bins and treated with Jackknife resampling, details about this process can be found in the Appendix. In my Monte Carlo simulation I introduced a variable that turns periodic boundary conditions on/off for a given direction of the lattice. This is important for the observables, which we are interested in. Specifically the surface-surface and surface-bulk correlation observables can only be calculated in systems with at least one surface, hence a site with non-periodic boundaries. Whether periodic boundaries are turned on/off for a specific direction, the length of the cubic lattice in each dimension is still fixed to the length L. This length L is equal in all directions. In this thesis I will always work with simulations where either all sides have periodic boundary conditions, or all except two ($\pm z$).

4.1.2 Validity of the simulation

In order to prove that my simulation is working and generating correct results, I compared e.g. the susceptibility χ

$$\chi = \frac{1}{L^3} \left\langle \left(\sum_x s_x \right)^2 \right\rangle \tag{22}$$

at high temperatures with values calculated using the high temperature expansion up to $20th$ order, from the paper[4]. This expansion is done for $D = 0.641$, so I used this value for my simulation as well in this case. I found the following

β	$\chi_{measured}$	χ_{HT}	Deviation in %	Deviation in σ_χ
0.3	3.14567(9951)	3.57713	12.06	4.34
0.2	1.21427(2333)	1.31429	7.61	4.29
0.12	0.80714(1436)	0.83992	3.90	2.28
0.1	0.76951(1379)	0.76786	0.22	0.12
0.08	0.69045(1344)	0.70640	2.26	1.19

Table 1: $D = 0.641$, $L = 32$, periodic boundary conditions in all directions

values (see Table 1). I noticed that for smaller values of β, thus higher temperatures, the value for χ improves drastically and approaches the theoretical value of the high temperature expansion up to $0.12\sigma_\chi$ in the case of $\beta = 0.1$. This makes sense since a high-temperature expansion is obviously only useful for small β. In comparison, the value for $\beta = 0.08$ is a bit more off, even though the β is smaller than 0.1, but with $1.19\sigma_\chi$ it is still in a reasonable range. I also compared the value of the Binder cumulant U_4 at $\beta_c(0.655)$ with the estimate from Hasenbusch's paper[8] for $D = 0.655$:

$$U_4 = 1.6036(1). \tag{23}$$

Since the Binder cumulant is universal, the value for the Ising model and Blume-Capel model should be the same in the limit $L \to \infty$. Although we can expect very similar values for finite lattice sizes already as we will see below. The reason for choosing the Binder cumulant is that, in the limit $L \to \infty$ the Binder cumulant becomes increasingly narrow, and is thus perfect for finding the critical temperature. A plot of it can be seen in Fig. 4.

$$U_4 = \frac{\langle M^4 \rangle}{\langle M^2 \rangle^2} \tag{24}$$

where

$$M = \sum_x s_x. \tag{25}$$

In the limit of $D \to -\infty$ we retrieve the Ising model (cf. Eq. 20). So if we set D to a small enough negative number, for example $D = -1000$, we should expect to see the phase transition at the critical temperature of the Ising model, with the same value for U_4. The critical temperature of the Ising model is[8]:

$$\beta_{c,Ising} = 0.22165463(8). \tag{26}$$

I conducted both simulations to further check the validity of my simulation and received the following results (see Table 2 and 3).
Considering the presence of finite-size effects the values still agree with the given estimate (Eq. 23) within the uncertainties very well. This is just an estimate from one simulation each for a (small) lattice size of $L = 32$, while the cited

β_c	U_4	Deviation in %	Deviation in σ_{U_4}
0.387721735	1.5865(223)	1.07	0.767

Table 2: $D = 0.655$, $L = 32$, periodic boundary conditions in all directions

$\beta_{c,Ising}$	U_4	Deviation in %	Deviation in σ_{U_4}
0.22165463	1.59206(1098)	1.72	2.023

Table 3: $D = -1000$, $L = 32$, periodic boundary conditions in all directions

paper used lattices up to a size of $L = 360$. It is not necessary to invest huge amounts of CPU hours to calculate these values for a bigger lattice, as smaller lattice sizes already give us a safe estimate whether the program works or not. So with these checks it is safe to say, that my code provides good results and is a valid simulation of the Blume Capel model (Eq. 19).

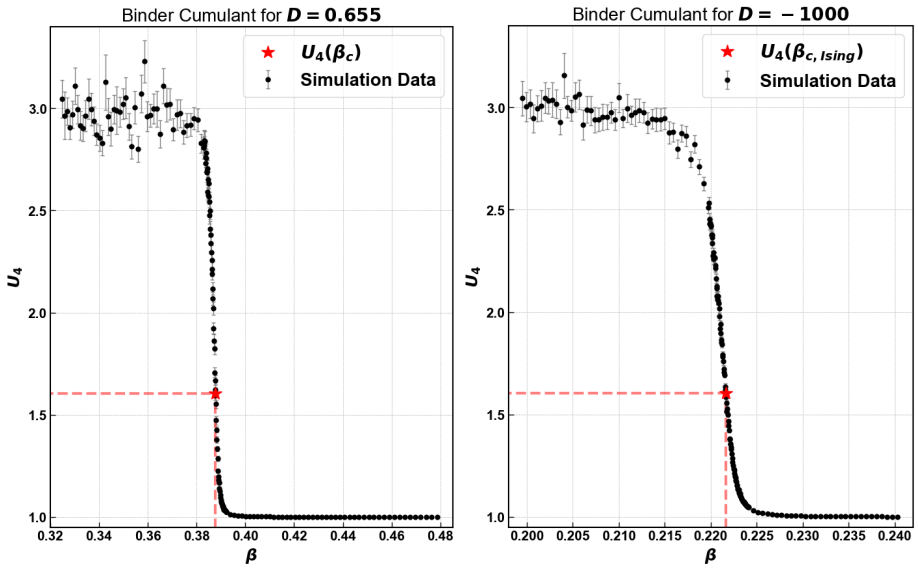

(a) β_c(0.655) (b) $\beta_{c,ising}$(-1000)

Figure 4: Visualisation of the phase transition, using the Binder cumulant for the Blume-Capel model at (a) $D = 0.655$ and (b) $D = -1000$, with $L = 32$

4.2 Observables and expansions

The goal of this thesis is to calculate the amplitudes of three different correlation functions:

1. The *surface* - *bulk* correlation amplitude
2. The *surface* - *surface* correlation amplitude
3. The *bulk* - *bulk* correlation amplitude for the case of perioidic boundaries in all directions

Generally the two-point correlation function is defined in the following way[13],

$$\Gamma(r) = \langle \rho(0)\rho(r) \rangle \tag{27}$$

with r as the spatial dimension between the two points at which the quantity ρ is measured. In the next three sections I will discuss the two-point functions for each of these three individual cases. I will measure those at the critical point, so we can expect to see power-law like behaviour. Since we can not generate infinite lattice sizes, there will be an expansion of each of these, which includes finite-size corrections. These will be the actual functions I will fit the data to later.

4.2.1 Surface-bulk correlation

The first two-point correlation function I will discuss is the two-point surface-bulk correlation function. This only works for a system with at least one surface. Since the system is translatation- and rotation-invariant it does not matter which direction we choose to have a surface. Here I chose the z-direction to have open boundary conditions in either direction $\pm z$, so there are two surfaces. My code calculates this sum once on each surface and then averages over both. In my code I have implemented this in the following way,

$$\Gamma_{SB}(z) = \left\langle \frac{1}{2L^2} \left(\sum_{x,y} s(x,y,0)s(x,y,z) + s(x,y,L)s(x,y,L-z) \right) \right\rangle \tag{28}$$

where $s(x,y,0)$ is a site on the two-dimensional surface (our reference point) and $s(x,y,z)$ any other site in the bulk. Since we sum over all spins on the surface, we normalise the function by dividing with L^2 and the $\frac{1}{2}$ comes from taking the mean over both surfaces. The $\langle\rangle$ brackets mean that we take the average over the entire Monte Carlo simulation and in each step I calculate this function for each $z \in \{1, ..., L\}$. We expect to see this correlation function to be proportional to some power-law, with amplitude $\mathcal{A}_\phi$:

$$\Gamma_{SB}(z) = \mathcal{A}_\phi z^{-\Delta}. \tag{29}$$

The finite size correction term is $\propto B_\phi$ in the function we are fitting to. It is derived from the operator product expansion. We also include another term $\propto$

F that covers scaling corrections[17]:

$$\Gamma_{SB}(z) = \mathcal{A}_\phi (z+z_0)^{-\Delta_B - \Delta_S} \left(1 + B_\phi \left(\frac{z+z_0}{L}\right)^3 + F(z+z_0)^{-2}\right). \quad (30)$$

In this function (Eq. 30), there is also a shift parameter z_0. The four parameters, I am estimating with the fit, are $\{z_0, A_\phi, B_\phi, F\}$. The operator product expansion exponents Δ_S[10] and Δ_B[12], which are the Δ in Eq. (29), are:

1. $\Delta_S = 1.2751(6)$
2. $\Delta_B = 0.5181489(10)$

4.2.2 Surface-surface correlation

The second two-point correlation function we are interested in, is the surface-surface two-point correlation function. This function gives us the correlation between two spins on a surface, seperated by the distance $y \in \{1, ..., L\}$. We calculate this function parallel to the calculation of the surface-bulk correlation function, as it also requires non-periodic boundary conditions on at least one surface. Although here we have two surfaces and take the average over both. I implemented it in my code, in the following way:

$$\Gamma_{SS}(y) = \left\langle \frac{1}{2L} \left(\sum_x s(x,0,0)s(x,y,0) + s(x,0,L)s(x,y,L) \right) \right\rangle. \quad (31)$$

Similarly as in the surface-bulk case, the spin $s(x,0,0)$ is a site on a surface, but is now limited on to a one-dimensional line in the x-direction (the reference point). The correlation is then the sum over each of the spins on this line, multiplied with the spin $s(x,y,0)$ in distance y on the surface and then normalised by dividing with L and the factor of $\frac{1}{2}$ comes from taking the average over both surfaces. We, again, take the average over the whole amount of Monte Carlo steps, where for each step we calculate the function at distance y. We also expect some power-law proportional behaviour here as well, with amplitude $\mathcal{S}_\phi$:

$$\Gamma_{SS}(y) = \mathcal{S}_\phi y^{-\Delta}. \quad (32)$$

Including the finite size and scaling corrections[17] we get the formula:

$$\Gamma_{SS}(y) = \mathcal{S}_\phi y^{-2\Delta_S}(1 + D_\phi \left(\frac{y}{L}\right)^3 + Cy^{-2}). \quad (33)$$

In this case we have three parameters, which we are fitting to: $\{\mathcal{S}_\phi, D_\phi, C\}$ the Δ_S which came from $\Delta = 2\Delta_S$ is the same as for the surface-bulk case $\Delta_S = 1.2751(6)$.

4.2.3 Bulk-bulk correlation

The final two-point correlation function we are interested in is the bulk-bulk two point correlation function. It gives us the correlation between two spins with distance r inside the bulk of our lattice. In this case there are only periodic boundary conditions and thus no surfaces. I implemented it in the following way

$$\Gamma_{BB}(r) = \left\langle \frac{1}{6L^3} \sum_{\mathbf{r}'} \sum_{\hat{\mathbf{e}}} \sum_{\pm} s(\mathbf{r}') s(\mathbf{r}' \pm r\hat{\mathbf{e}}) \right\rangle, \tag{34}$$

where $\hat{\mathbf{e}} \in \{(1,0,0),(0,1,0),(0,0,1)\}$ and $\sum_{\pm}$ means that we sum in both the positive and negative direction. The $\frac{1}{6}$ ensures that we are taking the average value of the correlation at distance r - averaged over all 6 directions ($\pm$) and $\sum_{\mathbf{r}'}$ ensures the summation over the whole cubic lattice. So contrary to the previous usage of $s(x,y,z)$ we generalise this here using $s(\mathbf{r}')$ where each vector $\mathbf{r}'$ denotes a lattice site, $\mathbf{r}' = (x,y,z)$. The values r can take are $r \in \{1,...,L\}$, although to be precise values greater than L can be calculated as well but due to periodic boundaries, the function just wraps around the lattice and we actually get the value for $\Gamma_{BB}(r \bmod L)$ - so it only makes sense to simulate it up to $r = L$. Here we can - again - expect power-law proportional behaviour, with amplitude $\mathcal{N}_\beta$:

$$\Gamma_{BB}(r) = \mathcal{N}_\beta r^{-\Delta}. \tag{35}$$

The expansion which takes finite size and scaling corrections into account, is the following:

$$\Gamma_{BB}(r) = \mathcal{N}_\beta r^{-2\Delta_B} \left(1 + B_\epsilon \left(\frac{r}{L}\right)^{\Delta_\epsilon} + G r^{-2}\right). \tag{36}$$

Where $\Delta_\epsilon = 1.412625(10)$, as found in[12]. Here the critical exponent is $\Delta = 2\Delta_B$, with $\Delta_B = 0.5181489(10)$ as in the surface-bulk case. So in this case we are fitting to three parameters $\{\mathcal{N}_\beta, B_\epsilon, G\}$.

4.3 Update algorithms

Update algorithms are a fundamental element of my Monte Carlo simulation. They are the technical cause that bring the system into a realistic representation of the model at set conditions. In the following two sections I will briefly explain the Metropolis- and Wolff algorithm and why I use them in my simulation.

4.3.1 Metropolis algorithm

The Metropolis algorithm is used to perform single-spin-flips. When the system is in thermal equilibrium, the energy fluctuates around a small range[2]. The Metropolis algorithm could be thought of as a vague representation of those fluctuations because a single-spin-flip is equivalent to a small fluctuation in energy.

Although in reality this is not exactly how complex systems work, since the interactions are a lot more complex than just the influence of nearest neighbours. By including this algorithm we introduce dynamics into our system. These dynamics propagate the system through a multitude of states until it emerges to a realistic representation at set parameters. It also guarantees ergodicity since we repeatedly apply this algorithm on random spins inside our cubic lattice. The Metropolis algorithm is defined and implemented in the following way (more details can be found in the Appendix):

1. Choose a random spin inside the cubic lattice.
2. When the spin is ± 1 we choose with 50% probability if it will be flipped to ∓ 1 or 0.
3. If the chosen spin is 0, we choose with 50% probability if it will be flipped to 1 or -1.
4. Flip the spin and calculate the resulting change in Energy ΔE.
5. If $\Delta E < 0$, accept the flip.
6. If $\Delta E > 0$, accept the flip with probability $e^{-\beta \Delta E}$.
7. Repeat until the system is in thermal equilibrium.

Here the way ΔE is calculated depends on the value of the initial spin. If the initially chosen spin had a value $s_0 \neq 0$, and is proposed to flip to a value $s_0' = -s_0$, then ΔE is calculated in the following way:

$$\Delta E_{s_0 \neq 0 \to s_0' = -s_0} = 2 s_0 \sum_{\langle y(s_0) \rangle} s_y \tag{37}$$

where $\langle y(s_0) \rangle$ means that only the sum over the (up to six) nearest neighbours of the initial spin s_0 is taken. If $s_0 \neq 0$, and is proposed to flip to zero $s_0' = 0$, then ΔE is calculated in the following way:

$$\Delta E_{s_0 \neq 0 \to s_0' = 0} = s_0 \sum_{\langle y(s_0) \rangle} s_y - D \tag{38}$$

If the initial spin has value $s_0 = 0$, then ΔE is calculated in the following way:

$$\Delta E_{s_0 = 0 \to s_0' \neq 0} = -s_0' \sum_{\langle y(s_0) \rangle} s_y + D \tag{39}$$

and is multiplied with the value s' that it will be (eventually) flipped to.
Of course if there are open boundaries, the sum $\sum_{\langle y(s_0) \rangle}$ will be smaller - since if s_0 is a spin on a surface, there are less neighbours.

4.3.2 Wolff algorithm

When the system approaches a critical point, we may notice an effect called *critical slowing down*. This effect leads to a divergence in the autocorrelation time, so we do not only notice large spatial correlations, but also large correlations in (Monte Carlo) time[22]. Cluster flipping algorithms, like the Wolff algorithm, flip entire clusters of spins at once, contrary to the Metropolis algorithm that does single local updates. This diminishes the long-range correlations and thus counteracts the critical slowing down. The Wolff algorithm is implemented in the following way[13]:

1. Choose a random spin inside the cubic lattice.
2. If the chosen spin is equal to zero, the algorithm breaks here. Otherwise we continue as follows.
3. We draw bonds to all nearest neighbours (with the same spin) with probability[4] $p = 1 - e^{-2K\delta_{s_x s_{x'}}}$.
4. If bonds have been drawn to any nearest neighbour, call that site x', we repeat step 3. and draw bonds to all nearest neighbours x'' of site x'. This happens again with the probability $p = 1 - e^{-2K\delta_{s_{x'} s_{x''}}}$.
5. Step 4. is repeated as long as no more new bonds are created.
6. Flip all spins in the cluster.

5 Numerical results

To calculate the amplitudes, I used a high-performance-cluster (HPC). The code used here, has slightly different parameters as the one I have written and discussed in section four.
Dr. Francesco Parisen Toldin is the author of the code used in this section. His code functions on parallel computing architectures by making use of e.g. the *Boost*:*MPI* library. I always used 48 cores on one node, but I will discuss the precise amount of nodes per lattice in the next section. On each core, the same simulation was run in parallel and the results of each run were then merged together to get better statistics.

5.1 Simulation parameters

I have collected the amount of nodes and Monte Carlo steps per lattice size in Table 4 and Table 5, where in each case 48 cores have been used. Each independent task used a different seed for the random generator. Contrary to my simulation, the Metropolis algorithm here does not choose random spins

[4] $K \equiv \frac{\mathcal{J}}{k_B T} = \frac{1}{T}$

L	Nodes	MC Steps
12	1	100.000
16	1	100.000
24	1	100.000
32	1	100.000
48	4	30.000
64	1	25.000
96	-	-
128	-	-
192	-	-

Table 4: Amount of nodes and Monte Carlo steps per simulation in the case of periodic boundaries.

L	Nodes	MC Steps
12	1	100.000
16	1	100.000
24	1	100.000
32	1	100.000
48	4	100.000
64	1	100.000
96	1	100.000
128	4	12.500
192	4	12.500

Table 5: Amount of nodes and Monte Carlo steps per simulation in the case of open boundaries.

inside the lattice, but runs through each spin once, in a *typewriter* like fashion. The value of β is tuned to the critical point[9] $\beta_c = 0.387721735$. The surface-coupling, which is $\beta \equiv \beta\mathcal{J}_s$ with $\mathcal{J}_s = 1$, is set to the same value. By tweaking the surface-coupling one could simulate other types of transitions, for example the special transition.
The rest is exactly as described in the previous section, just that this code provides more precise statistics due to the amount of tasks running in parallel. This is amplified by the possibility of a bigger amount of Monte Carlo steps, due to more efficient code and the usage of the cluster in general. Of course here we also discard the first 20% of values generated.

5.2 Statistical Treatment of the Fits

We can not assume statistical independence between points at a given lattice size, because they originate from the same Monte Carlo simulation. So in order to properly calculate the uncertainties on the fit parameters, I proceed in the following way[18]:
The χ^2 has to be minimized if we want to find the best fit. In the following I used the Jackknife method to calculate the χ^2 as well as an uncertainty for it. Consider a set of Monte Carlo estimates $\{O_i\}$, the Jackknife bin estimate is $\{O_i^J\}$, which is calculated using all Monte Carlo data except the discarded bin J. In the case of $N_{bins} = 100$, which is the case here, that equals to 100 sets of Jackknife bin estimates. A fit is conducted for each one of these data bins. So we receive 100 fits, where each provides a single Jackknife estimate (Eq. 59) of the fit-parameters $\{p_i^J\}$ and a $(\chi^2)^J$:

$$(\chi^2)^J = \sum_i \left(\frac{O_i^J - f(\{O_i^J\}, \{p_i^J\})}{\sigma_i^2} \right)^2 \tag{40}$$

Using these values, I calculate $\chi^2 = \overline{(\chi^2)^J}$ with Eq. 61 and the uncertainty can be calculated using Eq. 71. In Eq. 40 the σ_i is the estimate of the uncertainty of O_i, resulting from the appliance of the standard Jackknife routine. The σ_i is also used as input in the algorithm of the fit. Lastly I take the Jackknife average of all the 100 Jackknife estimates $\{p_i^J\}$ so that I get the final estimate $\overline{\{p_i^J\}}$ with uncertainties calculated using Eq. 71. In this case though the leading bias was not subtracted and is thus of order $1/N$ but this is negligible (see Eq. 65) [18].

5.3 Fit results

In the following I will present the results from the various fits I have conducted. The strategy behind finding a proper range for the distance used in the fits, is by finding the *asymptotic range*. The asymptotic range is the range in which the rescaled value of some correlation Γ(x), generally denoted as $\Gamma(x) \cdot x^{\Delta}$, is representing an asymptote. Since we assume that the correlation functions we are interested in here, follow a power-law like behaviour (cf. e.g. Eq. 32), by multiplying with that power-law we would expect to see an asymptote. The problem is that, as already mentioned, finite size effects and scaling corrections exist. So this asymptotic behaviour is only to be found in a small range, depending on the lattice size L. Only inside this range, the later introduced and estimated universal boundary operator product expansion coefficient μ is universal and thus it is important to properly estimate this range.
This range can be depicted using three parameters. In the surface-bulk case these are z_{min}, $(z/L)_{max}$ and L_{min}, where z_{min} stands for the minimum distance to the surface, $(z/L)_{max}$ gives the maximum value for z, depending on the lattice size L and L_{min} is the minimum lattice size that is included in this fitting algorithm.
That means for the (surface-bulk) fits we would in this case consider the range $\{z_{min}, ..., (z/L)_{max}\}$ of datapoints, for each lattice L [18].

5.3.1 Surface-Bulk: Γ_{SB}

In the folowing I fit the data (for open boundaries), calculated using Eq. 28 during the simulation, to Eq. 30:
As we can see in Fig. 5 the finite size effects are very strong in the case of Γ_{SB}. In the case of $L = 12 - 24$ there is hardly any asymptotic behaviour to be seen at all. With bigger lattice sizes we notice how the asymptotic is slowly being approached. I decided to not include the values of $L_{min} = 12, 16$ as the finite-size effects clearly dominate.
In the case of $L = 128$ one could roughly approximate that the asymptotic begins to end around $z \gtrapprox 20 - 25$. If we choose a range of at least $(z/L)_{max} = 1/8$, we would (for $L = 128$) include values up to $z = 16$. This would be a very safe assumption as we would definitely pick data points from the asymptotic range.
The z_{min} which depicts the start of the asymyptotic range, is a little harder to see, so after conducting a series of fits and checking their χ^2, I estimate it to be between $z_{min} = 4 - 8$ by looking at Fig. 5.
The estimates for $\mathcal{A}_\phi$ used in the determination of the final value can be found in Table 6. This table shows the best fits (determined by the value of $\chi^2/d.o.f.$). In the appendix a table with the remaining possibilities of z_{min}, $(z/L)_{max}$ and L_{min} can be found (Table 9).
The uncertainties in both tables include the dependence of the fits on varying Δ_B and Δ_S within their uncertainties.

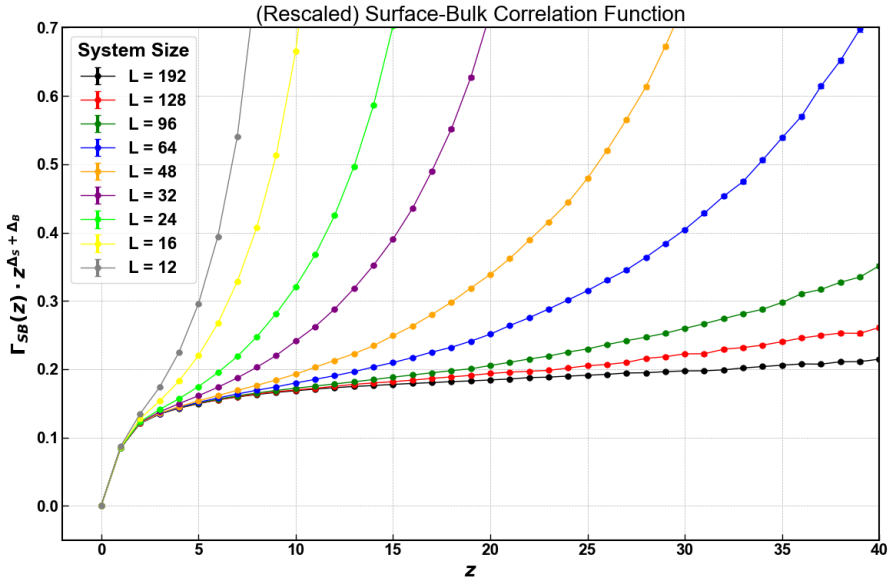

Figure 5: **Surface-Bulk:** Plot showing the *asymptotic range* of the rescaled correlation function $\Gamma_{SB}(z) \cdot z^{\Delta_S + \Delta_B}$.

z_{min}	$(z/L)_{max}$	L_{min}	$\mathcal{A}_\phi$	z_0	B_ϕ	F	χ^2/d.o.f.
4	$\frac{1}{8}$	48	0.1992(13)	1.172(43)	14.179(436)	3.664(354)	2.38(72)
		64	0.1987(13)	1.153(45)	15.069(642)	3.514(366)	2.10(62)
		96	0.1976(15)	1.108(50)	16.992(1.14)	3.151(391)	1.80(47)
		128	0.1987(18)	1.154(67)	15.409(1.961)	3.529(549)	1.18(44)
	$\frac{1}{12}$	96	0.1981(16)	1.140(54)	20.092(1.714)	3.445(433)	1.69(51)
		128	0.1993(21)	1.184(78)	15.517(3.982)	3.790(658)	1.54(56)
5	$\frac{1}{8}$	48	0.1976(14)	1.072(49)	14.532(460)	2.670(396)	1.67(64)
		64	0.1972(14)	1.062(50)	15.264(643)	2.609(398)	1.42(55)
		96	0.1961(16)	1.012(57)	17.193(1.186)	2.226(433)	0.96(39)
	$\frac{1}{12}$	64	0.1961(16)	1.015(58)	18.067(1.227)	2.237(437)	1.12(59)
		96	0.1960(16)	1.021(58)	19.843(1.683)	2.321(438)	0.71(49)
6	$\frac{1}{8}$	48	0.1971(17)	1.041(69)	14.616(534)	2.358(607)	1.41(59)
		64	0.1971(17)	1.050(70)	15.164(659)	2.481(615)	1.19(51)
		96	0.1960(19)	1.007(78)	16.952(1.216)	2.155(662)	0.75(33)
7	$\frac{1}{8}$	64	0.1972(21)	1.059(106)	15.048(710)	2.576(1.045)	1.00(47)
		96	0.1966(23)	1.046(110)	16.584(1.224)	2.577(1.063)	0.58(29)
8	$\frac{1}{8}$	64	0.1971(26)	1.054(147)	15.242(908)	2.530(1.571)	0.91(42)
		96	0.1972(27)	1.084(149)	16.321(1.256)	3.042(1.621)	0.56(28)

Table 6: **Surface-Bulk:** These are the results of various fits, which are used in the final determination of the value for $\mathcal{A}_\phi$.

5.3.2 Surface-Surface: Γ_{SS}

Here I fit the data (for open boundaries), calculated using Eq. 31 during the simulation, to Eq. 33:
In Fig. 6 we notice that the range of the fit $\{y_{min}, ..., (y/L)_{max}\}$ will be around the same range as in the **surface-bulk** case. We also notice from the plot, that $y_{min} \gtrapprox 4$. So the procedure is the same as in the **surface-bulk** case, and overall the fits perform best for $(y/L)_{max} = 1/8, 1/12$. The lattices $L = 128, 196$ were run for 12500 MC steps on four nodes each (as seen in Table 5), this is statistically equivalent to 50.000 steps each. Due to this fact, the statistics are worse, compared to the other simulations. I plotted both these lattices in Fig. 8, where one can see the magnitude of the uncertainties in comparison to $L = 96$, which was run for 100.000 steps. Although apart from this, it seems that this correlation function generally needs higher precision for increasing y. This is the reason why I chose not to include $(y/L)_{max} = 1/4$ in my fitting procedure. The uncertainties here also include the dependence of the fits on varying Δ_S within its uncertainty. The results used in the final determination of $\mathcal{S}_\phi$ can be found in Table 7. The remaining, not used values can be found in the Appendix under Table 10.

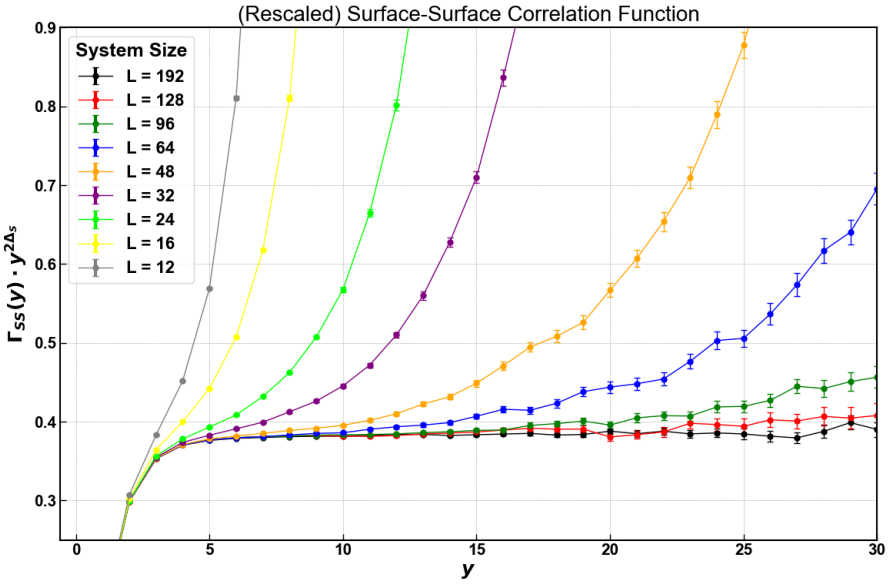

Figure 6: **Surface-Surface:** Plot showing the *asymptotic range* of the rescaled correlation function $\Gamma_{SS}(y) \cdot z^{2\Delta_S}$.

y_{min}	$(y/L)_{max}$	L_{min}	$\mathcal{S}_\phi$	C	D_ϕ	χ^2/d.o.f.
5	$\frac{1}{8}$	48	0.3841(15)	-0.490(45)	3.401(509)	1.15(47)
		64	0.3842(15)	-0.499(46)	2.740(870)	1.12(47)
		96	0.3840(15)	-0.486(46)	4.023(1.58)	1.12(46)
		128	0.3839(15)	-0.489(49)	4.792(3.341)	1.01(51)
	$\frac{1}{12}$	64	0.3841(15)	-0.499(44)	4.253(1.362)	1.66(82)
		96	0.3838(15)	-0.477(49)	6.960(2.631)	1.46(70)
		128	0.3838(16)	-0.481(52)	7.554(6.029)	1.40(86)
6	$\frac{1}{8}$	48	0.3836(17)	-0.425(79)	3.176(581)	0.92(41)
		64	0.3837(17)	-0.437(81)	2.762(889)	0.91(43)
		96	0.3833(18)	-0.392(85)	4.553(1.577)	0.77(36)
		128	0.3832(18)	-0.396(92)	6.260(3.423)	0.78(37)
	$\frac{1}{12}$	96	0.3831(18)	-0.389(85)	6.587(2.67)	1.00(57)
		128	0.3829(20)	-0.374(100)	10.459(6.306)	0.99(55)
7	$\frac{1}{8}$	64	0.3838(20)	-0.457(135)	2.868(912)	0.75(35)
		96	0.3834(21)	-0.396(146)	4.091(1.606)	0.68(34)
		128	0.3830(22)	-0.354(159)	6.345(3.494)	0.74(34)
	$\frac{1}{12}$	96	0.3833(21)	-0.405(143)	5.237(2.81)	0.98(57)
		128	0.3827(23)	-0.339(169)	9.707(6.543)	1.01(53)
8	$\frac{1}{12}$	96	0.3835(24)	-0.409(241)	4.186(3.1)	0.76(47)
		128	0.3831(28)	-0.353(281)	6.391(6.802)	0.81(51)

Table 7: **Surface-Surface:** These are the results of various fits, which are used in the final determination of the value for $\mathcal{S}_\phi$.

5.3.3 Bulk-Bulk: Γ_{BB}

Finally we are considering the data from the periodic boundaries case. Here I fit the data, calculated using Eq. 34 during the simulation, to Eq. 36.
The plot of the rescaled correlation function can be seen in Fig. 7, which shows that the finite-size effects are noticeable here as well. In this case, I only have the data for the lattice sizes $L = 12 - 64$ due to technical issues with the HPC cluster. I am discarding the data for $L = 12$, due to the finite-size effects which are very strong in this case as seen in the plot. One could argue that $L = 16$ could also be left out, but I leave it as the minimum possible L_{min} as I only have the data for five bigger lattice sizes. The best $(\chi^2/d.o.f.)$ values are found for $(r/L)_{max} = 1/4$. The $r_{min} = 3 - 7$ as in this range the $\chi^2/d.o.f.$ seemed reasonable inside its uncertainties. In the case of $r_{min} > 7$ the fits performed a lot worse and are thus left out. The results of the fits used in the final determination of $\mathcal{N}_\beta$ can be found in Table 8. A table including the case $(r/L)_{max} = 1/2$ can be found in the Appendix under Table 11.
Note: For this case the exponents Δ_B and Δ_ϵ have not been varied within their uncertainties, as this does not result in huge differences due to the high accuracy of these values in general.

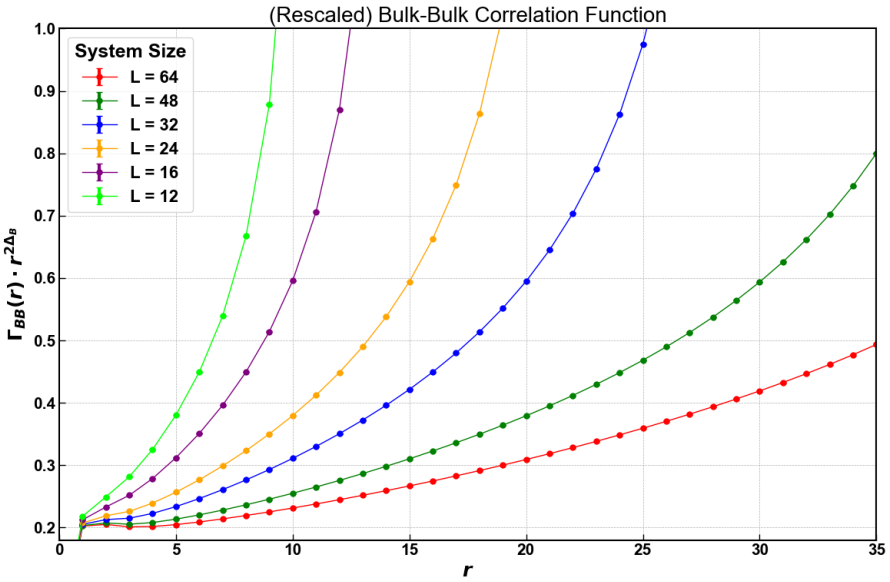

Figure 7: **Bulk-Bulk:** Plot showing the *asymptotic range* of the rescaled correlation function $\Gamma_{BB}(r) \cdot r^{2\Delta_B}$.

r_{min}	$(r/L)_{max}$	L_{min}	$\mathcal{N}_\beta$	B_ϵ	G	χ^2/d.o.f.
3	$\frac{1}{4}$	16	0.1846(2)	3.442(10)	0.384(7)	2.77(86)
		24	0.1845(2)	3.455(12)	0.392(8)	2.28(88)
		32	0.1842(2)	3.480(12)	0.406(8)	0.97(57)
		48	0.1841(1)	3.488(11)	0.412(5)	0.41(54)
4	$\frac{1}{4}$	16	0.1846(3)	3.453(14)	0.369(18)	1.31(78)
		24	0.1846(3)	3.457(17)	0.373(21)	1.32(79)
		32	0.1842(3)	3.482(20)	0.400(24)	0.73(58)
		48	0.1841(3)	3.491(20)	0.415(20)	0.42(63)
5	$\frac{1}{4}$	24	0.1844(4)	3.470(20)	0.373(42)	0.90(79)
		32	0.1841(5)	3.490(28)	0.409(53)	0.63(62)
		48	0.1839(6)	3.502(35)	0.439(61)	0.43(63)
6	$\frac{1}{4}$	24	0.1841(5)	3.491(24)	0.418(72)	0.63(73)
		32	0.1838(7)	3.506(34)	0.455(93)	0.52(60)
		48	0.1835(10)	3.523(55)	0.509(140)	0.38(51)
7	$\frac{1}{4}$	32	0.1834(8)	3.525(38)	0.542(144)	0.39(54)
		48	0.1830(14)	3.545(75)	0.620(259)	0.31(36)

Table 8: **Bulk-Bulk:** Detailed results for various r_{min} values. These are the results used to determine the final value for $\mathcal{N}_\beta$.

5.4 Final field theory coefficients

The (empirical) strategy I use to extract a final value for the amplitudes, out of my data sets is the following:
First I choose the fits which have a good enough $\chi^2/d.o.f.$, within its uncertainty. These fits can be found in the tables discussed above. Now, I look for the value of the given amplitude, that after subtracting its uncertainty, has the lowest possible value in the list. I do the same thing for the maximum value as well. By doing this I find a range in which the real value will most likely be found. So the final value I receive will be the *center* of this range and the uncertainty then would cover exactly that range. In the case of the **bulk-bulk** correlation it would look like this for $\mathcal{N}_\beta$. The minimum value is found for $r_{min} = 7$, $(r/L)_{max} = 1/4$ and $L_{min} = 48$:

$$\mathcal{N}_\beta^- = 0.1830 - 0.0014 = 0.1816 \tag{41}$$

The maximum value is found for $r_{min} = 4$, $(r/L)_{max} = 1/4$ and $L_{min} = 16, 24$:

$$\mathcal{N}_\beta^+ = 0.1846 + 0.0003 = 0.1849 \tag{42}$$

The final value that includes $\mathcal{N}_\beta^-$ and $\mathcal{N}_\beta^+$ within its uncertainties is then:

$$\mathcal{N}_\beta = \frac{\mathcal{N}_\beta^+ + \mathcal{N}_\beta^-}{2} = 0.1833(17) \tag{43}$$

Considering that the $\chi^2/d.o.f.$ is 0.31(36) for the case of the value used as $\mathcal{N}_\beta^-$, this is a rather generous guess, as all other values with a $\chi^2/d.o.f.$ closer to one, lie slightly above with a smaller uncertainty. Nonetheless all the values agree with each other within their uncertainties, and thus this choice is justified.
One also notices the partly huge deviations between the results from the fits for B_ϕ (Table 6) and D_ϕ (Table 7). These values seem to be highly sensitive regarding the choice of range, specifically the upper limit $(z/L)_{max}$ and $(y/L)_{max}$.
Applying this method to $\mathcal{A}_\phi$ and $\mathcal{S}_\phi$ gives us the final estimates of our amplitudes:

1. $\mathcal{A}_\phi = 0.1978(37)$
2. $\mathcal{S}_\phi = 0.3831(28)$
3. $\mathcal{N}_\beta = 0.1833(17)$

So why exactly are these amplitudes so interesting for us?
The answer is that a certain combination of these is actually *universal*. In the context of *conformal field theory* (CFT) one can show that,

$$\mu = \frac{\mathcal{N}_\perp}{\mathcal{N}_{Bulk} \cdot \mathcal{N}_{Surf}} \tag{44}$$

where $\mathcal{N}_\perp = \mathcal{A}_\phi$, $\mathcal{N}_{Bulk} = \sqrt{\mathcal{N}_\beta}$, $\mathcal{N}_{Surf} = \sqrt{\mathcal{S}_\phi}$ and μ the universal boundary operator product expansion coefficient.
Let us assume we view our lattice at criticality ($T = T_C$) and for large distances. Under these circumstances one can express the *lattice observables* as a sum of CFT fields: Observable $\rightarrow \sum$ CFT-Fields. In our model there are two different types of fields, the **bulk-fields** ϕ_{Bulk} and the **surface-fields** ϕ_{Surf}.
We can now expand a surface spin in terms of surface fields up to the leading term ϕ_{Surf} and $\vec{x} = (x, y)$

$$s(\vec{x}, z = 0) = \sum_i \mathcal{N}_{Surf}^i \phi_{Surf}^i(\vec{x}) \approx \mathcal{N}_{Surf} \phi_{Surf}(\vec{x}), \tag{45}$$

which has the lowest dimension Δ_S, where $\mathcal{N}_{Surf}$ is a non-universal normalization constant. The same would work for a spin located in the bulk as well, with $\mathcal{N}_{Surf} \rightarrow \mathcal{N}_{Bulk}$ for the lowest dimension Δ_B.
Now imagine we are deep inside the bulk and we begin to approach a surface, so $z \rightarrow 0$. At some point we will be able to express ϕ_{Bulk} to leading order in terms of ϕ_{Surf}

$$\phi_{Bulk}(\vec{x}, z)|_{z\rightarrow 0} = \sum_i C_i(\vec{x}, z) \phi_{Surf}^i(\vec{x}), \tag{46}$$

where the leading term of C_i for finite $|\vec{x}|$ and small z, can be written as

$$C_i(\vec{x}, z) = \mu_i \cdot z^{\Delta_{\phi_S} - \Delta_{\phi_B}} D^{\Delta_{\phi_S}}(z^2 \nabla^2), \tag{47}$$

where the differential operator D depends on Δ_{ϕ_S}, z^2 and $\nabla^2 = \partial_x^2 + \partial_y^2$. So the leading term ($D = 1$, see Eq. 7.3 in [15]) of Eq. 47 is

$$C_i(\vec{x}, z) \approx \mu_i \cdot z^{\Delta_{\phi_S} - \Delta_{\phi_B}}. \tag{48}$$

The correlation function between two surface-fields ϕ_{Surf}, has the following form:

$$\left\langle \phi_{Surf}(\vec{x})\phi_{Surf}(\vec{0}) \right\rangle = \frac{1}{|\vec{x}|^{2\Delta_{\phi_S}}}, \tag{49}$$

where for our model, $\Delta_{\phi_S} = \Delta_S = 1.2751(6)$ is the operator product expansion exponent. In the case of a correlation function between two bulk-fields ϕ_{Bulk} this exponent would change to $\Delta_B = 0.5181489(10)$.
Now multiplying the leading term of Eq. 46 by $\phi_{Surf}(\vec{0})$ we get

$$\phi_{Bulk}(\vec{x}, z)\phi_{Surf}(\vec{0}) \approx \mu \cdot z^{\Delta_{\phi_S} - \Delta_{\phi_B}} D^{\Delta_{\phi_S}} (z^2\nabla^2)\phi_{Surf}(\vec{x})\phi_{Surf}(\vec{0}). \tag{50}$$

Now by taking the expectation value of Eq. 50, it can be shown that[15]

$$\left\langle \phi_{Bulk}(\vec{x}, z)\phi_{Surf}(\vec{0}) \right\rangle \approx \mu \cdot \frac{z^{\Delta_{\phi_S} - \Delta_{\phi_B}}}{(x^2 + y^2 + z^2)^{\Delta_{\phi_S}}} \tag{51}$$

and then Eq. 51 for $\vec{x} = \vec{0}$ has the form

$$\left\langle \phi_{Bulk}(\vec{0}, z)\phi_{Surf}(\vec{0}) \right\rangle = \mu \cdot \frac{1}{z^{\Delta_{\phi_S} + \Delta_{\phi_B}}}. \tag{52}$$

So by substituting Δ_{ϕ_S} and Δ_{ϕ_B} with Δ_S and Δ_B we now understand why the correlation functions from our simulation follow these specific power-laws. In fact what we actually measure during the simulation corresponds to (with $\vec{r} = (x, y, z)$):
Surface-Bulk:

$$\Gamma_{SB} \mathrel{\widehat{=}} \mathcal{N}_{Bulk} \cdot \mathcal{N}_{Surf} \left\langle \phi_{Bulk}(\vec{0}, z)\phi_{Surf}(\vec{0}) \right\rangle = \mathcal{N}_{\perp} \left\langle \phi_{Bulk}(\vec{0}, z)\phi_{Surf}(\vec{0}) \right\rangle \tag{53}$$

Surface-Surface:

$$\Gamma_{SS} \mathrel{\widehat{=}} \mathcal{N}_{Surf}^2 \left\langle \phi_{Surf}(\vec{x})\phi_{Surf}(\vec{0}) \right\rangle \tag{54}$$

Bulk-Bulk:

$$\Gamma_{BB} \mathrel{\widehat{=}} \mathcal{N}_{Bulk}^2 \left\langle \phi_{Bulk}(\vec{r})\phi_{Bulk}(\vec{0}) \right\rangle \tag{55}$$

Finally using Eq. 53 we conclude Eq. 44. So indeed, what we measure during our simulation are the amplitudes $\mathcal{A}_\phi = \mathcal{N}_\perp$, $\mathcal{S}_\phi = \mathcal{N}_{Surf}^2$ and $\mathcal{N}_\beta = \mathcal{N}_{Bulk}^2$. The values of the normalization constants are then:

1. $\mathcal{N}_\perp = 0.1978(37)$
2. $\mathcal{N}_{Surf} = 0.6190(23)$
3. $\mathcal{N}_{Bulk} = 0.4281(20)$

The final value for μ, which now results from Eq. 44, is:

$$\mu = 0.746(14). \tag{56}$$

6 Conclusion and outlook

To conclude this thesis, I have successfully estimated the amplitudes of the discussed correlation functions. Using these amplitudes I have found an estimate of $\mu = 0.746(14)$, which was the ultimate goal of this thesis.
There were a few technical difficulties with the HPC-Cluster, due to which I was not able to run the simulation for $L > 64$ with periodic boundaries. Therefore the statistics are not ideal. Nonetheless my next goal is to expand on this problem using simulations of bigger lattice sizes and more Monte Carlo steps. In that way I will be able to fine-tune the value for μ. It is a great opporunity, as there is no precise estimate published yet.
By adjusting the surface-enhancement one could also study the special transition or other types of transitions. This is something that could be done in another project in the future.

Despite all the technical issues I encountered, I am very greatful that I had the opportunity to write this thesis, as I have truly learned a lot and I am looking forward to expand my knowledge further in this field.

A Jackknife resampling

The following two sections are based on "Everything you wanted to know about Data Analysis and Fitting but were afraid to ask" by Peter Young[23].
In the analysis of my numerical data, I assume that generally the correlation between my datapoints is negligible after some *relaxation time*. This relaxation time can be understood as some amount of Monte Carlo steps. So in order to truly generate (almost) uncorrelated datapoints I am splitting my data into bins of a fixed size. The binsize is chosen to be bigger than the relaxation time, so that neighbouring bins of data can be assumed to be uncorrelated. This is crucial, because if we want to obtain uncertainties on our datapoints, they have to be statistically independent of each other.
If we want to find the *true mean* of a distribution μ, we need to generate many sets of N data points and take the average of each set. These averages, also called sample averages, then take the form of the actual distribution. The more repetitions we do, the more preciesely we are averaging over the exact distribution and hence can find the true mean of that distribution. This is what we are doing when conducting Monte Carlo simulations.
But in order to present proper scientific data, we also need uncertainties. These can become very complicated to calculate as soon as we consider non-linear functions of (true) averages $f(\mu_x, \mu_y)$. The procedure is called error propagation (detailed procedure on the derivation can be found in the mentioned reference: [23]). One finds that the best estimate for the uncertainty σ_f of our non-linear function f is calculated using a handful of partial derivatives

$$\sigma_f^2 \approx \frac{1}{N-1}\left[(\partial_{\mu_x} f)^2 s_x^2 + 2(\partial_{\mu_x} f)(\partial_{\mu_y} f) s_{xy}^2 + (\partial_{\mu_y} f)^2 s_y^2\right], \tag{57}$$

where s_x^2 and s_y^2 are the average sample variances of the variables x and y and s_{xy}^2 the sample covariance of both variables. The uncertainty σ_f here is of order $\frac{1}{\sqrt{N}}$ as one can see in Eq. 57. That means our value becomes for example ten times more precise if we were to generate a hundred times as much data. This can be easily generalised to functions with more averages as arguments.
Luckily there exists the so-called *Jackknife - resampling* method. This method makes sure that the *resampling* of data automatically takes care of error propagation, without having to calculate all the partial derivatives, variances and covariances.
Consider a dataset of N datapoints. The $i-th$ jackknife estimate y_i^J is the average across all our datapoints, except one point - the point i:

$$y_i^J \equiv \frac{1}{N-1}\sum_{j\neq i} y_j. \tag{58}$$

Using this equation, we *resample* our dataset into N jackknife estimates of our variable. The corresponding jackknife estimate of the function $f(\mu_x, \mu_y)$ is then simply:

$$f_i^J \equiv f(x_i^J, y_i^J). \tag{59}$$

So instead of the sample averages, we use the jackknife estimates as arguments. One example could be the Binder ratio (Eq. 24) which I calculated to validate my simulation:

$$f_i^J = \frac{(N-1)^{-1}\sum_{j\neq i} x_j^4}{\left[(N-1)^{-1}\sum_{j\neq i} x_j^2\right]^2}. \tag{60}$$

Formula Eq. 60 shows how the jackknife estimate of the Binder ratio would be calculated. Now to calculate the overall jackknife estimate of $f(\mu_x, \mu_y)$, we simply take the average over all N jackknife estimates f_i^J, which we calculated using Eq. 58, in the following way:

$$\overline{f^J} \equiv \frac{1}{N}\sum_{i=1}^{N} f_i^J. \tag{61}$$

The last thing we are now interested in, is how to calculate the uncertainties here. We expand the function $f(\overline{x}, \overline{y})$ of our sample averages $\overline{x}$ and $\overline{y}$ around the (true) averages μ_x and μ_y (over many repetitions) and rearange the equation:

$$f(\mu_x, \mu_y) = \langle f(\overline{x}, \overline{y})\rangle - \frac{A}{N} - \frac{B}{N^2} + ..., \tag{62}$$

where A is $\frac{1}{2}$ times the term inside the brackets in Eq. 57 and B the next order correction. In the next step we replace the sample averages with the jackknife averages. Here we have to keep in mind, that the jackknife data sets have $N-1$ datapoints, so we need to replace $N \to N-1$ in Eq. 62 as well. The jackknife data sets follow the same distribution as the data sets with N values and the bias will also have the same form. Since the higher order terms A/N and B/N^2 represent that bias, their values will stay the same:

$$f(\mu_x, \mu_y) = \overline{\langle f^J\rangle} - \frac{A}{N-1} - \frac{B}{(N-1)^2} + ... \tag{63}$$

By creating a linear combination of $f(\overline{x}, \overline{y})$ and $\overline{f^J}$

$$f(\mu_x, \mu_y) = N\langle f(\overline{x}, \overline{y})\rangle - (N-1)\overline{\langle f^J\rangle} + \mathcal{O}(\frac{1}{N^2}), \tag{64}$$

one finds, that in order to eliminate the leading bias one should estimate $f(\mu_x, \mu_y)$ from $\left[Nf(\overline{x}, \overline{y}) - (N-1)\overline{f^J}\right]$. This means we do not even have to calculate any partial derivatives.
Although in this case the bias would be of order $1/N^2$, which is very small. So instead of doing that one could approximate $f(\mu_x, \mu_y)$ using just $f(\overline{x}, \overline{y})$ or the jackknife average $\overline{f^J}$. If this is done, the leading bias would be of order $1/N$, which is smaller than the statistical error that is of order $1/\sqrt{N}$. Because we choose our N *large enough* in our simulations, we can assume that the difference

$$|f(\overline{x}, \overline{y}) - \overline{f^J}| \ll \sigma_f \tag{65}$$

is a lot smaller than the uncertainty of $f(\mu_x, \mu_y)$. Because of this it is not necessary to eliminate the leading bias and we use the Jackknife average $\overline{f^J}$ as a good estimate of $f(\mu_x, \mu_y)$.
The variance of the jackknife averages is defined as:

$$s^2_{f^J} = \overline{(f^J)^2} - (\overline{f^J})^2 \tag{66}$$

with

$$\overline{(f^J)^2} = \frac{1}{N}\sum_{i=1}^{N}(f_i^J)^2. \tag{67}$$

Next we expand $\overline{f^J}$ at μ_x and μ_y up to the leading contribution, using Eq. 59, Eq. 61, Eq. 58 and rearrange:

$$\overline{f^J} - f(\mu_x, \mu_y) \approx (\partial_{\mu_x} f)(\overline{x} - \mu_x) + (\partial_{\mu_y} f)(\overline{y} - \mu_y). \tag{68}$$

The same can be done for $\overline{(f^J)^2}$ where the details for this and Eq. 68 can be found in the reference [23].
Using the results from Eq. 68 and Eq. 66, we find the variance in the jackknife estimates:

$$s^2_{f^J} = \frac{1}{(N-1)^2}\left[(\partial_{\mu_x} f)^2 s_x^2 + (\partial_{\mu_y} f)^2 s_y^2 + 2(\partial_{\mu_x} f)(\partial_{\mu_y} f) s_{xy}^2\right]. \tag{69}$$

This corresponds to $1/(N-1)\sigma_f^2$, where σ_f^2 is given in Eq. 57 and so the jackknife estimate for σ_f is,

$$\sigma_f = \sqrt{N-1}\, s_{f^J} \tag{70}$$

where s_{f^J} is the sample variance of the jackknife estimates. So ultimately in the algorithm the jackknife estimate of the uncertainty σ_f is calculated as follows (Eq. 71):

$$\sigma_f = \sqrt{\frac{N-1}{N}}\sum_{i=1}^{N}(f_i^J - \overline{f^J})^2. \tag{71}$$

A.1 Binning of Data

As already mentioned in the previous section, I chose to bin my data. The reason for this was that we need to be certain our datapoints are uncorrelated. The bin-size is thus chosen to be greater than the *relaxation time*, in which case neighbouring bins can be assumed to be uncorrelated. This is roughly the case for $N_{Bin} \approx 100$. The way this is implemented in the analysis is the following:

1. Bin the data into N_{Bin} bins.
2. Calculate the average value of each bin.
3. Treat these averages like individual (uncorrelated) data points inside the Jackknife method:

(a) Calculate the Jackknife estimates using Eq. 58.

(b) Calculate the Jackknife average using Eq. 61.

(c) Calculate the Jackknife estimate of the uncertainty using Eq. 71.

Of course in these equations N has to be replaced by the new amount of datapoints N_{Bin}.

B Extra remarks about the Metropolis algorithm

This section is based on section 4.2.1 from Prof. David P. Landau's and Prof. Kurt Binder's book "A Guide to Monte Carlo Simulations in Statistical Physics (Fifth Edition)"[13]. Inside the Metropolis algorithm, the configurations which are being generated, are all based on the state the system has been in before. More generally said, it is used to create a Markov chain of states, based on the Boltzmann distribution, where the leading state x_{i+1} is always only dependent on the previous state x_i.
Consider the following example of the Ising model[11]. In this case one can imagine the chain of states that is generated to follow a time ordered, non-deterministic path, also called *Monte Carlo time*. The *standard* Monte Carlo time is usually measured in an attempt of flipping every spin in the system once, so basically one Monte carlo step. The behaviour of this model can be described by the following equation:

$$\frac{\partial P_n(t)}{\partial t} = -\sum_{n \neq m} \left[P_n(t) W_{n \to m} \; - P_m(t) W_{m \to n} \right], \tag{72}$$

with $P_n(t)$ as the probability of the system being in state n at the time t and $W_{n \to m}$ as the transition rate from the state $n \to m$. If both terms in the sum on the right side of Eq. 72 are equal, then $\partial P_n(t)/\partial t = 0$ and the system is said to be in *equilibrium*[13].
Now the Metropolis algorithm generates canonical states of our system (because the temperature is constant). So the probability for the n^{th} state to occur inside a classical system is given by:

$$P_n(t) = \frac{1}{Z} e^{-E_n/k_B T}. \tag{73}$$

But the problem is that it is very difficult to calculate the partition function.
The solution is to generate a Markov chain of states, where as already mentioned the leading state x_{i+1} is generated from the previous state x_i. In this case let us say we go from state $m \to n$. We can calculate the relative probability of this happening in the following way:

$$\frac{P_n(t)}{P_m(t)} = \frac{e^{-E_n/k_B T}}{e^{-E_m/k_B T}} \frac{Z}{Z} = e^{-\beta(E_n - E_m)} = e^{-\beta \Delta E}. \tag{74}$$

We notice that by doing this, the partition function cancels and the relative probability is only dependent on ΔE.
From the *equilibrium condition* we get the *detailed balance* equation:

$$P_n(t)W_{n\to m} = P_m(t)W_{m\to n}. \tag{75}$$

So as long as the detailed balance is satisfied, any transition rate is accepted.

$$W_{m\to n} = \tau_0^{-1} e^{-\beta\Delta E}, \quad \Delta E > 0 \tag{76}$$

$$W_{m\to n} = \tau_0^{-1}, \quad \Delta E < 0 \tag{77}$$

Now, one usually choses $W_{m\to n}$ to be τ_0^{-1} for $\Delta E < 0$ and Eq. 76 for $\Delta E > 0$, where τ_0^{-1} is the *time* required to propose a spin-flip, but this is set to $\tau_0^{-1} = 1$. So this is the reason why the transition probabilities are the way they are and it makes physically sense to accept a new configuration with *less* energy with a rate/probability of 1 (Eq. 77)[13].
There is one last comment concerning the Metropolis algorithm:
It generally takes a bunch of Monte carlo steps, until the system is fully thermalized. This is because we start with a random configuration of spins, this would technically represent a system of infinite temperature. So through the iteration of the Metropolis algorithm inside our Monte Carlo simulation we get closer to the actual configuration at the temperature we defined our system to be at. This is - again - due to the Metropolis algorithm creating canonical states at constant temperature. So by undergoing small energy changes in the form of single spin-flips we slowly but steadily get to our desired configuration. The reason is simply that in the beginning of the simulation basically every flip-proposal is accepted with practically 100% probability. The consequence of that is, that the first x configurations of the system will not belong to the actual temperature we are interested in. This is the fundamental reason why I discard the first 20% of the generated data[13].

C Data tables and more

z_{min}	$(z/L)_{max}$	L_{min}	$\mathcal{A}_\phi$	z_0	B_ϕ	F	χ^2/d.o.f.
4	$\frac{1}{4}$	24	0.2027(12)	1.308(43)	10.858(157)	4.818(399)	7.04(1.09)
		32	0.2022(12)	1.295(46)	11.365(183)	4.738(424)	4.58(82)
		48	0.2009(13)	1.236(45)	12.105(235)	4.201(402)	2.95(59)
		64	0.2005(13)	1.221(46)	12.318(282)	4.056(404)	2.73(61)
		96	0.2001(13)	1.206(48)	12.666(371)	3.935(410)	2.32(58)
		128	0.2005(14)	1.234(50)	12.554(447)	4.214(442)	1.25(47)
	$\frac{1}{12}$	48	0.1989(15)	1.161(52)	15.608(795)	3.581(427)	2.92(90)
		64	0.1988(15)	1.162(52)	16.904(1.171)	3.599(427)	2.60(76)
5	$\frac{1}{4}$	24	0.2014(13)	1.221(48)	11.076(171)	3.846(434)	6.54(1.04)
		32	0.2013(13)	1.233(51)	11.477(193)	4.042(474)	4.36(81)
		48	0.2001(14)	1.184(53)	12.199(248)	3.633(474)	2.74(56)
		64	0.1996(14)	1.155(53)	12.473(300)	3.353(465)	2.45(57)
		96	0.1989(15)	1.124(57)	12.952(407)	3.082(484)	1.95(52)
		128	0.1992(15)	1.153(59)	12.945(489)	3.365(516)	1.02(42)
	1/12	128	0.1969(23)	1.050(85)	15.703(4.3)	2.493(657)	0.23(17)
6	$\frac{1}{4}$	24	0.2010(14)	1.189(62)	11.228(199)	3.478(590)	5.87(98)
		32	0.2013(15)	1.232(66)	11.456(214)	4.031(665)	4.14(81)
		48	0.2006(16)	1.218(71)	12.088(265)	4.025(711)	2.49(55)
		64	0.1998(16)	1.171(70)	12.407(316)	3.536(678)	2.27(55)
		96	0.1989(17)	1.124(77)	12.929(453)	3.078(727)	1.79(49)
		128	0.1994(18)	1.166(82)	12.889(553)	3.505(793)	1.04(43)
	$\frac{1}{12}$	96	0.1958(20)	0.999(81)	19.210(1.702)	2.104(676)	0.49(46)
		128	0.1965(27)	1.019(109)	15.553(4.353)	2.184(890)	0.20(18)
7	$\frac{1}{4}$	32	0.2012(17)	1.226(85)	11.476(248)	3.956(914)	3.84(79)
		48	0.2014(18)	1.281(96)	11.922(291)	4.839(1.079)	2.24(55)
		64	0.2005(19)	1.227(95)	12.270(337)	4.238(1.038)	2.09(54)
		96	0.1992(21)	1.147(105)	12.845(498)	3.340(1.085)	1.64(47)
		128	0.2000(22)	1.211(114)	12.732(623)	4.064(1.245)	1.05(45)
	$\frac{1}{12}$	96	0.1963(26)	1.031(127)	18.291(1.735)	2.421(1.204)	0.34(42)
		128	0.1971(32)	1.060(148)	15.347(4.344)	2.622(1.379)	0.21(19)
8	$\frac{1}{4}$	32	0.2012(20)	1.234(107)	11.597(293)	4.071(1.236)	3.25(72)
		48	0.2020(21)	1.331(119)	11.785(320)	5.563(1.479)	2.13(56)
		64	0.2013(21)	1.292(123)	12.119(364)	5.157(1.508)	1.98(55)
		96	0.1994(24)	1.165(134)	12.780(536)	3.587(1.522)	1.58(46)
		128	0.1999(26)	1.201(153)	12.758(705)	3.926(1.801)	1.09(46)
	$\frac{1}{12}$	96	0.1961(34)	1.012(189)	18.211(1.999)	2.201(1.917)	0.39(45)
		128	0.1964(36)	1.014(189)	15.662(4.326)	2.107(1.871)	0.25(23)

Table 9: **Surface-bulk:** Remaining values of the various fits, which were **not** used in the determination of the final value for $\mathcal{A}_\phi$.

y_{min}	$(y/L)_{max}$	L_{min}	$\mathcal{S}_\phi$	C	$\mathcal{D}_\phi$	χ^2/d.o.f.
3	$\frac{1}{8}$	24	0.3895(10)	-0.839(10)	3.413(235)	41.52(5.21)
		32	0.3896(10)	-0.841(10)	2.905(360)	42.01(5.29)
		48	0.3899(10)	-0.846(10)	0.394(564)	40.14(5.41)
		64	0.3901(10)	-0.851(10)	-4.237(1.015)	37.11(5.07)
		96	0.3902(10)	-0.853(10)	-10.209(1.878)	35.04(4.76)
		128	0.3900(10)	-0.848(10)	-17.994(3.701)	32.87(4.66)
	$\frac{1}{12}$	48	0.3898(10)	-0.846(10)	2.547(763)	63.55(8.25)
		64	0.3901(10)	-0.850(10)	-2.962(1.336)	62.93(8.39)
		96	0.3905(10)	-0.858(10)	-17.358(2.903)	56.81(8.08)
		128	0.3906(10)	-0.861(10)	-42.919(6.172)	46.55(7.09)
4	$\frac{1}{8}$	32	0.3855(12)	-0.621(23)	3.671(355)	3.80(1.04)
		48	0.3856(12)	-0.625(23)	3.107(508)	3.71(1.08)
		64	0.3857(12)	-0.631(23)	1.681(886)	3.43(1.06)
		96	0.3857(12)	-0.630(23)	1.264(1.646)	3.50(1.12)
		128	0.3856(13)	-0.628(24)	-0.148(3.402)	2.88(1.06)
	$\frac{1}{12}$	48	0.3857(12)	-0.631(23)	3.251(803)	5.35(1.72)
		64	0.3857(12)	-0.630(23)	3.536(1.231)	5.56(1.78)
		96	0.3856(13)	-0.626(24)	3.453(2.671)	5.69(1.85)
		128	0.3858(13)	-0.635(24)	-3.855(5.905)	4.51(1.84)
8	$\frac{1}{8}$	64	0.3837(22)	-0.439(214)	3.336(1.044)	0.55(31)
		96	0.3835(24)	-0.406(240)	3.783(1.671)	0.56(31)
		128	0.3830(26)	-0.334(276)	5.825(3.729)	0.59(34)

Table 10: **Surface-Surface:** Remaining values of the various fits, which were **not** used in the determination of the final value for $\mathcal{S}_\phi$.

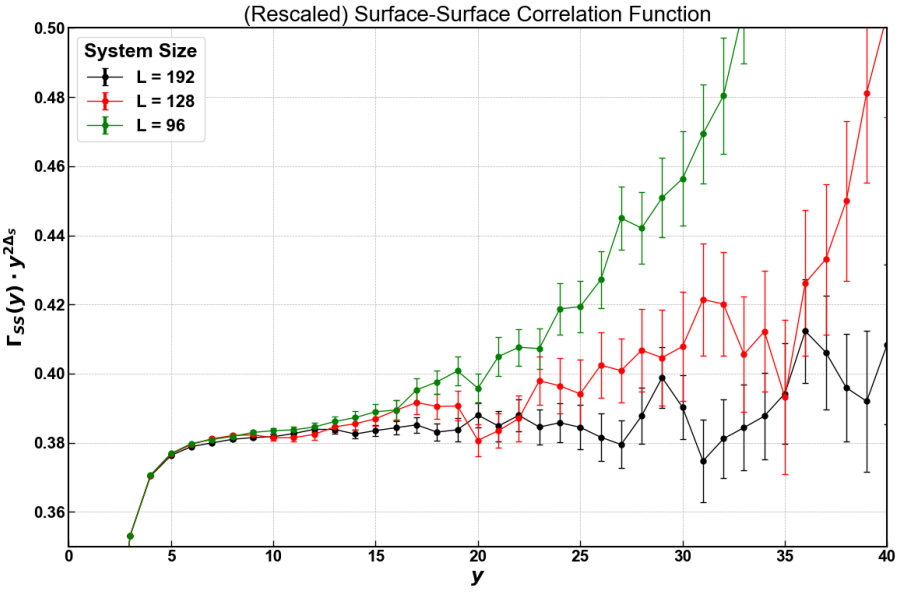

Figure 8: **Surface-Surface:** Plot showcasing the magnitude of uncertainties for large y.

r_{min}	$(r/L)_{max}$	L_{min}	$\mathcal{N}_\beta$	$\mathcal{B}_\epsilon$	G	χ^2/d.o.f.
3	$\frac{1}{2}$	16	0.1813(1)	3.731(6)	0.506(6)	90.89(1.69)
		24	0.1811(1)	3.744(6)	0.525(6)	73.73(1.63)
		32	0.1811(1)	3.749(5)	0.536(5)	57.29(90)
		48	0.1814(1)	3.732(7)	0.530(3)	45.94(50)
4	$\frac{1}{2}$	16	0.1803(2)	3.778(9)	0.607(18)	82.84(1.59)
		24	0.1799(2)	3.797(9)	0.662(18)	68.53(1.74)
		32	0.1796(2)	3.817(8)	0.722(15)	51.52(1.2)
		48	0.1798(1)	3.806(7)	0.733(9)	39.45(40)
5	$\frac{1}{2}$	16	0.1792(3)	3.829(12)	0.759(41)	74.49(1.48)
		24	0.1788(3)	3.846(13)	0.844(42)	64.26(1.74)
		32	0.1779(3)	3.886(12)	1.023(39)	47.36(1.53)
		48	0.1778(2)	3.893(9)	1.115(25)	33.69(65)
6	$\frac{1}{2}$	16	0.1778(4)	3.890(15)	1.003(77)	65.67(1.47)
		24	0.1777(4)	3.891(17)	1.046(84)	59.86(1.61)
		32	0.1763(4)	3.952(18)	1.420(84)	44.27(1.78)
		48	0.1755(3)	3.992(14)	1.736(59)	28.84(1.08)
7	$\frac{1}{2}$	16	0.1761(5)	3.964(19)	1.385(130)	57.24(1.55)
		24	0.1767(6)	3.937(22)	1.253(145)	54.66(1.37)
		32	0.1750(6)	4.009(25)	1.844(159)	41.78(1.85)
		48	0.1730(5)	4.096(21)	2.614(127)	25.25(1.55)

Table 11: **Bulk-Bulk:** Remaining values of the various fits, which were **not** used in the determination of the final value for $\mathcal{N}_\beta$.

References

[1] Stephen R. Addison. Homogenous functions in thermodynamics. *Journal of the Arkansas Academy of Science: Vol 45, Article 35*, 1992.

[2] G. T. Barkema and M. E. J. Newman. *Monte Carlo Methods in Statistical Physics*. Oxford University Press, U.S.A., 1999.

[3] M. Blume. Theory of the first-order magnetic phase change in uo22. physicsl review, 141(2), 517. 1966.

[4] Massimo Campostrini, Andrea Pelissetto, Paolo Rossi, and Ettore Vicari. Improved high-temperature expansion and critical equation of state of three-dimensional ising-like systems. *Physical Review E*, 60(4):3526–3563, October 1999.

[5] H.W. Capel. On the possibility of first-order phase transitions in ising systems of triplet ions with zero-field splitting. physica 32.5:966-988. *Physica*, 1966.

[6] John L Cardy. *Scaling and renormalization in statistical physics*. Cambridge lecture notes in physics. Cambridge Univ. Press, Cambridge, 1996.

[7] H. W. Diehl. The theory of boundary critical phenomena. *International Journal of Modern Physics B*, 11(30):3503–3523, December 1997.

[8] Martin Hasenbusch. Finite size scaling study of lattice models in the three-dimensional ising universality class. *Physical Review B*, 82(17), November 2010.

[9] Martin Hasenbusch. Monte carlo study of surface critical phenomena: The special point. *Physical Review B*, 84(13), October 2011.

[10] Martin Hasenbusch. Thermodynamic casimir force: A monte carlo study of the crossover between the ordinary and the normal surface universality class. *Physical Review B*, 83(13), April 2011.

[11] Kyozi Kawasaki and Tomoji Yamada. Time-Dependent Ising Model with Long Range Interaction. *Progress of Theoretical Physics*, 39(1):1–25, 01 1968.

[12] Filip Kos, David Poland, David Simmons-Duffin, and Alessandro Vichi. Precision islands in the ising and o(n) models. *Journal of High Energy Physics*, 2016(8), August 2016.

[13] David P. Landau and Kurt Binder. *A Guide to Monte Carlo Simulations in Statistical Physics*. Cambridge University Press, 2000.

[14] F. Léonard and B. Delamotte. Critical exponents can be different on the two sides of a transition: A generic mechanism. 115(20):200601, 2015.

[15] D.M. McAvity and H. Osborn. Conformal field theories near a boundary in general dimensions. *Nuclear Physics B*, 455(3):522–576, September 1995.

[16] Lars Onsager. Crystal statistics. i. a two-dimensional model with an order-disorder transition. *Phys. Rev.*, 65:117–149, Feb 1944.

[17] Francesco Parisen Toldin and Max A. Metlitski. Boundary criticality of the 3d o(n) model: From normal to extraordinary. *Phys. Rev. Lett.*, 128:215701, May 2022.

[18] Francesco Parisen Toldin and Max A. Metlitski. Boundary criticality of the 3d o(n) model: From normal to extraordinary (supplemental material). *Phys. Rev. Lett.*, 128:215701, May 2022.

[19] M. Saito and M. Matsumoto. Simd-oriented fast mersenne twister: a 128-bit pseudorandom number generator. 2008.

[20] Prof. Dr. Benjamin Simons. Lecture notes on phase transitions and collective phenomena, chapter 1: Critical phenomena. `https://www.tcm.phy.cam.ac.uk/~bds10/phase.html`. Accessed: 2024-02-09.

[21] Prof. Dr. Benjamin Simons. Lecture notes on phase transitions and collective phenomena, chapter 3: The scaling hypothesis. `https://www.tcm.phy.cam.ac.uk/~bds10/phase/scalin.pdf`. Accessed: 2024-02-12.

[22] Ulli Wolff. Collective monte carlo updating for spin systems. 1988.

[23] Peter Young. Everything you wanted to know about data analysis and fitting but were afraid to ask, 2014.